Published for SISSA by Springer

Received: *April 15, 2014*
Accepted: *April 25, 2014*
Published: *May 23, 2014*

A relation between screening masses and real-time rates

B.B. Brandt,[a] **A. Francis,**[b] **M. Laine**[c] **and H.B. Meyer**[b]

[a] *Institute for Theoretical Physics, University of Regensburg, 93040 Regensburg, Germany*

[b] *PRISMA Cluster of Excellence, Institute for Nuclear Physics, Helmholtz Institute Mainz, Johannes Gutenberg University Mainz, 55099 Mainz, Germany*

[c] *Institute for Theoretical Physics, Albert Einstein Center, University of Bern, Sidlerstrasse 5, 3012 Bern, Switzerland*

E-mail: bastian.brandt@physik.uni-regensburg.de, francis@kph.uni-mainz.de, laine@itp.unibe.ch, meyerh@kph.uni-mainz.de

Abstract: Thermal screening masses related to the conserved vector current are determined for the case that the current carries a non-zero Matsubara frequency, both in a weak-coupling approach and through lattice QCD. We point out that such screening masses are sensitive to the same infrared physics as light-cone real-time rates. In particular, on the perturbative side, the inhomogeneous Schrödinger equation determining screening correlators is shown to have the same general form as the equation implementing LPM resummation for the soft-dilepton and photon production rates from a hot QCD plasma. The static potential appearing in the equation is identical to that whose soft part has been determined up to NLO and on the lattice in the context of jet quenching. Numerical results based on this potential suggest that screening masses overshoot the free results (multiples of $2\pi T$) more strongly than at zero Matsubara frequency. Four-dimensional lattice simulations in two-flavour QCD at temperatures of 250 and 340 MeV confirm the non-static screening masses at the 10% level. Overall our results lend support to studies of jet quenching based on the same potential at $T \gtrsim 250\,\mathrm{MeV}$.

Keywords: Thermal Field Theory, Quark-Gluon Plasma, Resummation, Lattice QCD

ArXiv ePrint: 1404.2404

doi:10.1007/JHEP05(2014)117

JHEP05(2014)117

Contents

JHEP05(2014)117

1 Introduction

Even though an asymptotically free gauge theory at a temperature (T) much higher than the confinement scale is sometimes called weakly coupled, its dynamics is non-trivial. Denoting the gauge coupling by $g = \sqrt{4\pi\alpha_{\rm s}}$, such a theory possesses three parametrically different momentum scales [1]: πT, gT, and g^2T/π, with by assumption $\pi T \gg gT \gg g^2T/\pi$. The structure of any physical observable can be viewed in various ways:

(i) In a strict *weak-coupling expansion*, observables are computed in a power series in g. It is a consequence of the momentum scales as mentioned above that odd powers and logarithms of g appear [2, 3] and that some of the coefficients are non-perturbative [4]. It is also commonly believed that the series converges slowly unless g is extremely small, a problem often associated with the dynamics of the intermediate scale gT.

(ii) In an *effective theory approach* [5, 6], only the "hardest" scale is treated perturbatively. It is "integrated out" in order to derive an effective low-energy description for the "soft" scales gT and g^2T/π. The dynamics of the low-energy modes is solved non-perturbatively, often with the help of "dimensionally reduced" lattice simulations.

(iii) In principle the most precise level is a fully non-perturbative solution of a given problem, with methods of four-dimensional lattice QCD. A major practical limitation of this approach is that the simulations are carried out in the imaginary-time formalism. If real-time observables are to be considered, an analytic continuation is required, which in practice is ill-controlled (for a review, see ref. [7]).

There are many phenomenologically interesting observables in thermal QCD, notably screening masses and real-time rates such as the photon and dilepton production rates from the plasma, or the rate of "jet quenching" of energetic probes passing through the plasma, which are dominantly determined by the soft scale gT. Given the systematic uncertainties of the third approach, it is suggestive to also follow the second approach for the study of these observables. For screening masses related to flavour-singlet (gluonic) states, this approach leads to a good description of thermal QCD down to temperatures of a few hundred MeV [8]. Recently it has been proposed to apply the same approach to jet quenching [9], and indeed first simulation results exist already [10].

Nevertheless, it may be questioned with every observable how accurate the effective theory approach really is; certainly it breaks down at temperatures very close to the confinement scale, which it does not capture. The purpose of this paper is to elaborate on a non-trivial if indirect crosscheck: we point out that there is a class of Euclidean observables, namely flavour non-singlet (mesonic) screening masses at non-zero Matsubara frequency, which are sensitive to the same infrared physics as is relevant for jet quenching or photon and dilepton production. By measuring these observables on a 4-dimensional lattice and comparing with results based on the effective theory approach, we can lend credibility to the latter.

The screening masses related to mesonic operators are at leading order multiples of $2\pi T$, because of the boundary conditions imposed on quarks across the time direction. Corrections originate from a "potential" $V(r) \sim (g^2T/\pi)\,\phi(gTr, g^2Tr/\pi)$. The potential balances against a kinetic energy $\sim (1/\pi T)\partial_r^2$, so that the typical momentum scale probed is $1/r \sim \sqrt{g^2T^2} \sim gT$. Therefore it would be helpful to determine the function ϕ without recourse to any expansion, and this is what can be achieved with the second approach.

The plan of this paper is the following. After defining the correlators in section 2, we compute them in non-interacting QCD in section 3. In section 4 we show that the QCD results can be reproduced through an effective theory. The parameters of the effective theory are determined through matching computations in section 5, and in section 6 we recall how the solution of the problem within the effective theory reduces to a 2-dimensional Schrödinger equation. Numerical estimates following from this equation are displayed in section 7. A lattice calculation in two-flavor QCD is presented in section 8, where we also compare with the predictions following from the effective Schrödinger equation. An outlook and conclusions are offered in section 9.

JHEP05(2014)117

2 Basic definitions

Letting γ_μ denote Euclidean Dirac matrices, with $\{\gamma_\mu, \gamma_\nu\} = 2\delta_{\mu\nu}$ and $\gamma_\mu^\dagger = \gamma_\mu$, we consider the quark-connected (or flavour non-singlet) vector current correlator

$$G_{\mu\nu}^{(k_n)}(z) \equiv \int_0^{1/T} \mathrm{d}\tau\, e^{ik_n\tau} \int_{\mathbf{x}} \Big\langle (\bar\psi\gamma_\mu\psi)(\tau,\mathbf{x},z)(\bar\psi\gamma_\nu\psi)(0)\Big\rangle_{\mathrm{c}} \,, \tag{2.1}$$

where $k_n \equiv 2\pi n T$ is a bosonic Matsubara frequency, T is the temperature, and $\mathbf{x} \equiv (x_1, x_2)$ denotes a 2-dimensional vector in a "transverse" plane. A corresponding Fourier transform is formally defined as

$$G_{\mu\nu}^{(k_n)}(k_3) \equiv \int_{-\infty}^{\infty} \mathrm{d}z\, e^{ik_3 z}\, G_{\mu\nu}^{(k_n)}(z) \,. \tag{2.2}$$

It is also convenient to define a "spectral function" as

$$\rho_{\mu\nu}^{(k_n)}(\omega) \equiv \mathrm{Im}\, G_{\mu\nu}^{(k_n)}(k_3 \to -i[\omega + i0^+]) \,. \tag{2.3}$$

For $\mu = \nu$, $G_{\mu\nu}^{(k_n)}(z)$ is symmetric in $z \to -z$, so that $G_{\mu\nu}^{(k_n)}(k_3)$ is even and $\rho_{\mu\nu}^{(k_n)}(\omega)$ is odd in its argument. Then $G_{\mu\nu}^{(k_n)}(z)$ can be represented as a Laplace transform:

$$G_{\mu\nu}^{(k_n)}(z) \stackrel{\mu=\nu}{=} \int_0^\infty \frac{\mathrm{d}\omega}{\pi}\, e^{-\omega|z|}\, \rho_{\mu\nu}^{(k_n)}(\omega) \,. \tag{2.4}$$

The low-lying spectrum of $\rho_{\mu\nu}^{(k_n)}(\omega)$ is discrete; the corresponding energies, leading to an exponential falloff of $G_{\mu\nu}^{(k_n)}(z)$, are called screening masses.

Not all of the components of $G_{\mu\nu}^{(k_n)}$ are independent. Ward identities related to current conservation, $k_n G_{00}^{(k_n)} + k_3 G_{30}^{(k_n)} = 0$ and $k_n G_{03}^{(k_n)} + k_3 G_{33}^{(k_n)} = 0$, as well as the definition of a "longitudinal" correlator $G_L^{(k_n)} \equiv G_{00}^{(k_n)} + G_{33}^{(k_n)}$ which plays a role in dilepton production, lead to

$$G_L^{(k_n)}(k_3) = \frac{k_n^2 + k_3^2}{k_3^2}\, G_{00}^{(k_n)}(k_3) \,. \tag{2.5}$$

It is therefore sufficient to compute $G_{00}^{(k_n)}$, whose analysis turns out to be simpler than that of $G_{33}^{(k_n)}$ (cf. ref. [11]). Apart from $G_{00}^{(k_n)}$, we also consider the transverse part

$$G_T^{(k_n)}(k_3) \equiv \sum_{i=1}^{2} G_{ii}^{(k_n)}(k_3) \,, \tag{2.6}$$

which is not constrained by Ward identities.

Given that we have chosen a particular direction (z) in which to measure the correlators, it is convenient to choose a representation of the Dirac matrices which is commensurate with this choice. Starting with the standard (Euclidean) representation, this can be achieved through a transformation $\gamma_\mu \to U\gamma_\mu U^{-1}$, with a matrix U given in ref. [12]. After this transformation, the matrices $\gamma_0\gamma_\mu$ relevant for the "non-relativistic" effective description (cf. e.g. eq. (5.11)) read

$$\gamma_0 = \begin{pmatrix} 0 & 1 \\ 1 & 0 \end{pmatrix} , \quad \gamma_0^2 = \begin{pmatrix} 1 & 0 \\ 0 & 1 \end{pmatrix} , \quad \gamma_0\gamma_i = \epsilon_{ij} \begin{pmatrix} 0 & -\sigma_j \\ \sigma_j & 0 \end{pmatrix} , \quad \gamma_0\gamma_3 = \begin{pmatrix} i & 0 \\ 0 & -i \end{pmatrix} , \tag{2.7}$$

JHEP05(2014)117

where the blocks are 2×2-matrices, σ_j are Pauli matrices, and $\epsilon_{12} = 1$. Unless stated otherwise, latin indices take values labelling the transverse directions, $i, j \in \{1, 2\}$.

In a previous study [12], the screening masses of $G_T^{(k_n)}$ at $k_n = 0$, as well as similar results for scalar and pseudoscalar densities and the axial current, were determined up to next-to-leading order (NLO). All of the screening masses are equal in this approximation: $m = 2\pi T + cg^2 N_{\rm c} T/(2\pi)$, where c is a small positive coefficient whose value depends on the number of dynamical fermions. Numerical measurements (cf. refs. [13–15] and references therein) have detected discrepancies with respect to this prediction, particularly for the scalar and pseudoscalar channels where the results are clearly below $2\pi T$. Here we extend the study to $k_n \neq 0$, whereby the coefficient c and the quality of the comparison both change.

3 Leading-order computation in full QCD

Before considering NLO corrections, we work out the leading-order (LO) predictions. It turns out that analytic results can be given for the case that no average over the transverse directions is taken in eq. (2.1). Let us denote such correlators by

$$G_{\mu\nu}^{(k_n)}(\mathbf{r}) \equiv \int_0^{1/T} \mathrm{d}\tau\, e^{ik_n\tau} \Big\langle (\bar\psi\gamma_\mu\psi)(\tau,\mathbf{r})(\bar\psi\gamma_\nu\psi)(0) \Big\rangle_{\rm c} \,, \quad \mathbf{r} \equiv (\mathbf{x}, z) \,. \tag{3.1}$$

The correlators can be computed with the mixed coordinate space-momentum space techniques introduced in ref. [16]. In coordinate space, spatial propagators have the form

$$\int \frac{\mathrm{d}^3\mathbf{p}}{(2\pi)^3} \frac{e^{i\mathbf{p}\cdot\mathbf{r}}}{p_n^2 + p^2} = \frac{e^{-|p_n| r}}{4\pi r} \,, \quad r \equiv |\mathbf{r}| \,. \tag{3.2}$$

Subsequently one is faced with sums of the type

$$\sum_{\{p_n\}} e^{-|p_n| r - |p_n - k_n| r}\, P_\alpha(|p_n|) \,, \tag{3.3}$$

where $\{p_n\}$ denotes a fermionic Matsubara frequency and P_α is a polynomial of degree $\alpha \in \{0, 1, 2\}$. The sums can be carried out in analytic form, cf. e.g. ref. [17]. Denoting

$$\bar r \equiv 2\pi T r \,, \quad \frac{k_n}{2\pi T} = n \,, \tag{3.4}$$

we obtain (here $i, j \in \{1, 2, 3\}$)

$$-\frac{r^2 G_{00}^{(k_n)}(\mathbf{r})}{N_{\rm c} T^3 e^{-|k_n| r}} = \frac{|n|}{6} + \frac{|n|^3}{3} + \frac{|n|^2}{\bar r} + \frac{|n|}{\bar r^2} + \frac{|n|}{\bar r \sinh \bar r} + \frac{\cosh \bar r}{\bar r \sinh^2 \bar r} + \frac{1}{\bar r^2 \sinh \bar r} \,, \tag{3.5}$$

$$\begin{aligned} \frac{r^2 G_{ij}^{(k_n)}(\mathbf{r})}{N_{\rm c} T^3 e^{-|k_n| r}} = {} & \frac{r_i r_j}{r^2} \left(\frac{|n|}{6} + \frac{|n|^3}{3} + \frac{|n|^2}{\bar r} + \frac{|n|}{\bar r^2} + \frac{|n|}{\bar r \sinh \bar r} + \frac{\cosh \bar r}{\bar r \sinh^2 \bar r} + \frac{1}{\bar r^2 \sinh \bar r} \right) \\ & - \left(\delta_{ij} - \frac{r_i r_j}{r^2} \right) \left(\frac{|n|^2}{\bar r} + \frac{|n|}{\bar r^2} + \frac{|n|}{\bar r \sinh \bar r} + \frac{\cosh \bar r}{\bar r \sinh^2 \bar r} + \frac{1}{\bar r^2 \sinh \bar r} \right. \\ & \left. + \frac{|n| \cosh \bar r}{\sinh^2 \bar r} + \frac{1}{2 \sinh \bar r} + \frac{1}{\sinh^3 \bar r} \right) . \end{aligned} \tag{3.6}$$

JHEP05(2014)117

Structures with $\sinh\bar{r}$ in the denominator are exponentially suppressed at $\bar{r}\gg 1$; however they are relevant for $n=0$ in which case the other terms disappear. (For $n=0$ a similar expression for the pseudoscalar correlator was given in ref. [18]. NLO corrections could be worked out with the techniques introduced in ref. [19].)

Let us now take the transverse averages $\int_{\mathbf{x}}$. The powerlike terms can be integrated in terms of the exponential integral

$$E_1(z)\equiv\int_z^\infty \mathrm{d}t\,\frac{e^{-t}}{t}\overset{z\gg 1}{\approx}\frac{e^{-z}}{z}\left(1-\frac{1}{z}+\frac{2}{z^2}+\ldots\right), \tag{3.7}$$

yielding ($\bar{z}\equiv 2\pi T z$)

$$-\frac{G_{00}^{(k_n)}(z)}{2\pi N_{\rm c}T^3}=e^{-|n\bar{z}|}\,\frac{n^2}{2|\bar{z}|}\left(1+\frac{1}{|n\bar{z}|}\right)+E_1(|n\bar{z}|)\,\frac{|n|(1-n^2)}{6}+\mathcal{O}\Big(e^{-(|n|+1)|\bar{z}|}\Big)\,, \tag{3.8}$$

$$\begin{aligned}\frac{G_T^{(k_n)}(z)}{2\pi N_{\rm c}T^3}&=e^{-|n\bar{z}|}\left[\frac{|n|(n^2-1)(1-|n\bar{z}|)}{12}-\frac{n^2}{2|\bar{z}|}\left(1+\frac{1}{|n\bar{z}|}\right)\right]\\&\quad+E_1(|n\bar{z}|)\left[\frac{|\bar{z}^2n^3|(n^2-1)}{12}+\frac{|n|}{6}+\frac{|n^3|}{3}\right]+\mathcal{O}\Big(e^{-(|n|+1)|\bar{z}|}\Big)\,.\end{aligned} \tag{3.9}$$

The equations simplify greatly for $|n|=1$ (we also assume $z>0$ here):

$$G_{00}^{(\pm k_1)}(z)\,=\,-N_{\rm c}T^2\,\frac{e^{-\bar{z}}}{2z}\left(1+\frac{1}{\bar{z}}\right)+\mathcal{O}(e^{-2\bar{z}})\,, \tag{3.10}$$

$$G_T^{(\pm k_1)}(z)\,=\,-N_{\rm c}T^2\left[\frac{e^{-\bar{z}}}{2z}\left(1+\frac{1}{\bar{z}}\right)-\pi T E_1(\bar{z})\right]+\mathcal{O}(e^{-2\bar{z}})\approx-\frac{N_{\rm c}Te^{-\bar{z}}}{2\pi z^2}\,. \tag{3.11}$$

In order to gain an intuitive understanding, eqs. (3.10), (3.11) can be represented by spectral functions like in eq. (2.3). We obtain, for $\omega>0$,

$$\rho_{00}^{(k_1)}(\omega)\,=\,-N_{\rm c}T\,\theta(\omega-k_1)\,\frac{\omega}{4}+\mathcal{O}(\theta(\omega-k_2))\,, \tag{3.12}$$

$$\rho_T^{(k_1)}(\omega)\,=\,-N_{\rm c}T\,\theta(\omega-k_1)\,\frac{\omega^2-k_1^2}{4\omega}+\mathcal{O}(\theta(\omega-k_2))\,. \tag{3.13}$$

These results are reproduced below from a "low-energy description", valid for the regime $|\omega-k_1|\ll k_1$, but it is already clear that the physics corresponds to a 2-particle threshold, with a discontinuous ($\rho_{00}^{(k_1)}$) or continuous ($\rho_T^{(k_1)}$) spectral function.

We note that the asymptotic behaviours of eqs. (3.10), (3.11) contain a power-law in addition to an exponential decay. Physically, this corresponds to an approximation in which two *free* heavy particles are generated with a continuous spectrum; the extra suppression in eq. (3.11) compared with eq. (3.10) is due to the fact that the latter is a P-channel correlator. After interactions are taken into account, the particles are bound together, and the spectrum is discrete, $\rho(\omega)\sim\sum_n c_n\delta(\omega-\omega_n)$; therefore we expect that in the full theory there is no power correction to the exponential decay.

In the "static" sector, $k_n=0$, the roles of the two channels are interchanged. The spatially averaged correlators become

$$G_{00}^{(0)}(z)\,=\,-N_{\rm c}T^2\left[\frac{e^{-\bar{z}}}{z}\left(1+\frac{1}{\bar{z}}\right)-2\pi T E_1(\bar{z})\right]+\mathcal{O}(e^{-3\bar{z}})\approx-\frac{N_{\rm c}Te^{-\bar{z}}}{\pi z^2}\,, \tag{3.14}$$

JHEP05(2014)117

$$G_T^{(0)}(z) \,=\, -N_{\rm c}T^2\left[\frac{e^{-\bar{z}}}{z}\left(1+\frac{1}{\bar{z}}\right)+2\pi T E_1(\bar{z})\right]+\mathcal{O}(e^{-3\bar{z}}) \approx -\frac{2N_{\rm c}T^2e^{-\bar{z}}}{z}, \tag{3.15}$$

and the corresponding spectral functions read

$$\rho_{00}^{(0)}(\omega) \,=\, -N_{\rm c}T\,\theta(\omega-k_1)\,\frac{\omega^2-k_1^2}{2\omega}+\mathcal{O}(\theta(\omega-k_3))\,, \tag{3.16}$$

$$\rho_{T}^{(0)}(\omega) \,=\, -N_{\rm c}T\,\theta(\omega-k_1)\,\frac{\omega^2+k_1^2}{2\omega}+\mathcal{O}(\theta(\omega-k_3))\,. \tag{3.17}$$

4 Effective description

We now build an effective theory which allows us to describe the physics of the correlators considered around the threshold $\omega \sim \max(k_1,k_n)$ (we restrict to $k_n \geq 0$ without loss of generality). We start with a tree-level construction, and promote it to loop level in section 5.

The correlator of eq. (2.1) can be re-written as

$$G_{\mu\nu}^{(k_n)}(z) = T\int_{\mathbf{x}}\Big\langle V_\mu^{(k_n)}(\mathbf{x},z)V_\nu^{(-k_n)}(0)\Big\rangle_{\rm c}\,, \tag{4.1}$$

where after substituting $\bar{\psi}(\tau)=T\sum_{\{p_n\}}e^{-ip_n\tau}\bar{\psi}_{p_n}$, $\psi(\tau)=T\sum_{\{p_n\}}e^{ip_n\tau}\psi_{p_n}$,

$$V_\mu^{(k_n)}(\mathbf{x},z) = T\sum_{\{p_n\}}\bar{\psi}_{p_n}(\mathbf{x},z)\,\gamma_\mu\,\psi_{p_n-k_n}(\mathbf{x},z)\,. \tag{4.2}$$

In order to represent these operators within an effective theory, it is convenient to introduce an abelian source field B_μ which couples to eq. (4.2). This can be achieved by adding $S_B \equiv \int_0^{1/T}\mathrm{d}\tau\int_{\mathbf{x},z}\bar{\psi}\gamma_\mu B_\mu\psi$ to the original QCD action, with B_μ expressed in Matsubara modes as

$$B_\mu(\tau,\mathbf{x},z) \equiv \sum_{k_n} B_\mu^{(k_n)}(\mathbf{x},z)\,e^{ik_n\tau}\,. \tag{4.3}$$

The full action is $S\equiv S_{\rm QCD}+S_B$, where $S_{\rm QCD}$ is the part without B_μ. The vector currents and their correlators can then be derived from the identity

$$V_\mu^{(k_n)}(\mathbf{x},z) = \frac{\delta S_B}{\delta B_\mu^{(k_n)}(\mathbf{x},z)}\,. \tag{4.4}$$

The idea of the effective approach is dimensional reduction, i.e. keeping only the Matsubara zero modes of the SU(3) gauge fields in the covariant derivatives $D_\mu=\partial_\mu-igA_\mu$ (cf. ref. [20]). At tree-level, this means that we replace the original action through

$$S_{\rm QCD}\to S_0 \,\equiv\, \int_0^{1/T}\mathrm{d}\tau\int_{\mathbf{x},z}\bar{\psi}\,\gamma_\mu D_\mu^{(n=0)}\psi\,. \tag{4.5}$$

Making use of the representation of Dirac matrices in eq. (2.7) and denoting

$$\psi = \frac{1}{\sqrt{T}}\begin{pmatrix}\chi\\ \phi\end{pmatrix}\,, \tag{4.6}$$

we thereby get

$$S_0 = \sum_{\{p_n\}} \int_{\mathbf{x},z} \Big[i\chi^\dagger_{p_n}(p_n - gA_0 + D_3)\chi_{p_n} + i\phi^\dagger_{p_n}(p_n - gA_0 - D_3)\phi_{p_n} + \epsilon_{ij}\Big(\chi^\dagger_{p_n}\sigma_i D_j\phi_{p_n} - \phi^\dagger_{p_n}\sigma_i D_j\chi_{p_n}\Big)\Big] , \tag{4.7}$$

$$S_B = \sum_{\{p_n\},k_n} \int_{\mathbf{x},z} \Big[B_0^{(k_n)}\Big(\chi^\dagger_{p_n}\chi_{p_n-k_n} + \phi^\dagger_{p_n}\phi_{p_n-k_n}\Big) + iB_3^{(k_n)}\Big(\chi^\dagger_{p_n}\chi_{p_n-k_n} - \phi^\dagger_{p_n}\phi_{p_n-k_n}\Big) + B_i^{(k_n)}\epsilon_{ij}\Big(\phi^\dagger_{p_n}\sigma_j\chi_{p_n-k_n} - \chi^\dagger_{p_n}\sigma_j\phi_{p_n-k_n}\Big)\Big] . \tag{4.8}$$

From S_0 it is observed that free propagators,

$$\langle\chi_{p_n}(z_1)\chi^\dagger_{p_n}(z_2)\rangle \simeq \int_{p_3} e^{ip_3(z_1-z_2)}\frac{-i}{p_n+ip_3} , \quad \langle\phi_{p_n}(z_1)\phi^\dagger_{p_n}(z_2)\rangle \simeq \int_{p_3} e^{ip_3(z_1-z_2)}\frac{-i}{p_n-ip_3} , \tag{4.9}$$

are proportional to $\theta(z_1-z_2)$ for $\chi_{p_n>0}$ and $\phi_{p_n<0}$; and to $\theta(z_2-z_1)$ for $\chi_{p_n<0}$ and $\phi_{p_n>0}$. For any p_n one of the fields is thus "non-propagating" or "short-range" and can be integrated out. Given that fermionic fields appear quadratically, the integration out can equivalently be achieved by solving equations of motion. This yields the simplified representation

$$S_0 = \sum_{\{p_n\}} \int_{\mathbf{x},z} \Big[i\chi^\dagger_{p_n}\Big(p_n - gA_0 + D_3 - \frac{D_iD_i + i\sigma_3\epsilon_{ij}D_iD_j}{2p_n}\Big)\chi_{p_n} + i\phi^\dagger_{p_n}\Big(p_n - gA_0 - D_3 - \frac{D_iD_i + i\sigma_3\epsilon_{ij}D_iD_j}{2p_n}\Big)\phi_{p_n} + \mathcal{O}\Big(\frac{1}{p_n^2}\Big)\Big] . \tag{4.10}$$

Given that $\chi_{p_n<0}, \phi_{p_n>0}$ are non-propagating (we consider $z_1 > z_2$), forward-propagating mesons are of the types $\phi^\dagger_{p_n}\chi_{p'_n}$ and $\phi^\dagger_{p_n}\phi_{-p'_n}$ with $p_n, p'_n > 0$. It is seen from eq. (4.8) that $B_0^{(k_n)}$ and $B_3^{(k_n)}$ couple to operators of this type for $0 < p_n < k_n$. The transverse source $B_i^{(k_n)}$ couples to $\epsilon_{ij}\big(\phi^\dagger_{p_n}\sigma_j\chi_{p_n-k_n} - \chi^\dagger_{p_n}\sigma_j\phi_{p_n-k_n}\big)$ which is non-propagating for $0 < p_n < k_n$.[1] However, by making use of equations of motion for the non-propagating modes $\chi_{p_n-k_n}$ and $\chi^\dagger_{p_n}$, there is still a $1/p_n$ or $1/(k_n - p_n)$-suppressed projection to a forward-propagating mode:

$$V_i^{(k_n;p_n)} = \epsilon_{ij}\big(\phi^\dagger_{p_n}\sigma_j\chi_{p_n-k_n} - \chi^\dagger_{p_n}\sigma_j\phi_{p_n-k_n}\big) \tag{4.11}$$

$$= \phi^\dagger_{p_n}\left\{\left(\frac{1}{p_n} - \frac{1}{k_n-p_n}\right)\frac{\overleftrightarrow{D_i}}{4i} - \left(\frac{1}{p_n} + \frac{1}{k_n-p_n}\right)\frac{\sigma_3\epsilon_{ij}\overleftrightarrow{D_j}}{4}\right\}\phi_{p_n-k_n} + \mathcal{O}\Big(\frac{1}{p_n}, \frac{1}{k_n-p_n}\Big)^2 ,$$

where $\overleftrightarrow{D_j} \equiv \overrightarrow{\partial_j} - \overleftarrow{\partial_j} - 2igA_j$, and total derivatives were omitted. Therefore, the correlator $G_T^{(k_n)}$ is also non-zero; it is simply power-suppressed with respect to $G_{00}^{(k_n)}$.

Whereas the operators are of the type $\phi^\dagger_{p_n}\phi_{-p'_n}$ in the non-static sector, they are of the type $\phi^\dagger_{p_n}\chi_{p_n}$ in the static sector (i.e. for $k_n = 0$). For $V_i^{(0)}$ this is immediately visible

[1] The mode propagates for $p_n > k_n$, but then the coefficient of the exponential decay is $p_n + p'_n = 2p_n - k_n > k_n$, i.e. the contribution is exponentially suppressed at large distances.

JHEP05(2014)117

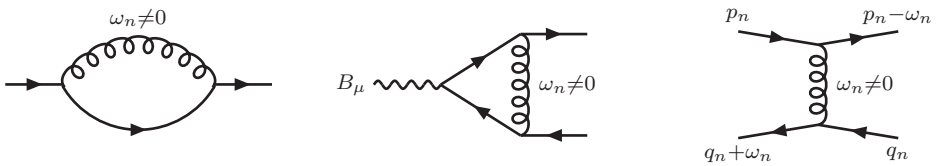

Figure 1. The graphs for determining the effective mass parameter (left), the effective coupling of the vector current to the low-energy modes (middle), as well as 4-quark operators (right).

from eq. (4.8), whereas for $V_0^{(0)}$ the elimination of non-propagating modes (separately for $p_n > 0$ and $p_n < 0$) yields

$$V_0^{(0;\,p_n)} = \chi^\dagger_{p_n}\chi_{p_n} + \phi^\dagger_{p_n}\phi_{p_n} = \frac{\epsilon_{ij}}{2ip_n}\left\{\phi^\dagger_{p_n}\sigma_i \overleftrightarrow{D}_j \chi_{p_n} - \chi^\dagger_{p_n}\sigma_i \overleftrightarrow{D}_j \phi_{p_n}\right\} + \mathcal{O}\left(\frac{1}{p_n^2}\right). \quad (4.12)$$

This is clearly a P-channel operator.

5 Mass and vertex corrections

In the discussion of the previous section, only Matsubara zero modes of gauge fields appeared. In full QCD, there are obviously also non-zero Matsubara modes. The description of eqs. (4.8), (4.10) should be viewed as a low-energy effective theory from which the non-zero Matsubara modes have been integrated out. The effect of the integration out is to modify the parameters of the low-energy description, and this is the topic of the present section.

Before proceeding, let us discuss the kinematic regime relevant for the problem. As became clear in section 3, for $k_n \neq 0$ the long-distance screening concerns a distance scale $z \sim 1/k_n$ and is therefore determined by the kinematic regime $K^2 = k_n^2 + k_3^2 \sim 0$. As was discussed in section 4 (cf. e.g. eq. (4.9)), the quark Matsubara modes are close to on-shell, with $P^2 = p_n^2 + p_3^2 \sim 0$. In a typical case (as discussed in more detail below) the two "constituents" have the Matsubara modes $p_n = k_n/2$. Therefore, even though we are considering a Euclidean problem, the kinematics is formally similar to that of collinear splitting, in which a nearly on-shell photon with Minkowskian four-momentum $\mathcal{K} = (k^0, \mathbf{k})$ splits into two fermions with four-momenta $\mathcal{P} = \mathcal{K}/2$. This formal similarity suggests a relationship of the current problem to that of photon ($\mathcal{K}^2 = 0$) or soft-dilepton ($\mathcal{K}^2 \sim g^2T^2$) production from a QCD plasma.

The similarity turns out to extend into practical computations, notably the determination of effects from non-zero Matsubara modes. Indeed, the mass and vertex corrections induced by the non-zero modes can be extracted from computations which are essentially equivalent to the derivation of the Hard Thermal Loop (HTL) effective action [21, 22]. The reason is that the assumptions needed in the computations are $K^2 \ll (\pi T)^2, P^2 \ll (\pi T)^2, (K-P)^2 \ll (\pi T)^2$, which as we have argued are true in our situation as well. The graphs to be considered are shown in figure 1, in which a 4-quark operator has been included as well (cf. ref. [20]).

JHEP05(2014)117

After computing the graphs and expanding to leading order in $K^2/(\pi T)^2, P^2/(\pi T)^2, (K-P)^2/(\pi T)^2$, the results can be expressed as corrections to the actions in eqs. (4.8), (4.10). Using for the moment the original fermion fields, the free part of S_0 becomes[2]

$$S_0 = \sum\!\!\!\!\!\!\int_{\{P\}} i\,\bar{\psi}(P)\biggl[\not{P} + \frac{m_\infty^2}{2}\int_v \frac{i\gamma_0 + \mathbf{v}\cdot\boldsymbol{\gamma}}{ip_n + \mathbf{v}\cdot\mathbf{p}}\biggr]\psi(P)\;, \tag{5.1}$$

where $P = (p_n, \mathbf{p})$, $\not{P} \equiv \gamma_\mu P_\mu$, $\mathbf{v}\cdot\boldsymbol{\gamma} \equiv v_i\gamma_i$, and $\int_v$ is the integral over directions of a unit vector ($|\mathbf{v}| = 1$), normalized as $\int_v 1 = 1$. The "asymptotic mass" parameter reads

$$m_\infty^2 \equiv \frac{g^2T^2C_{\rm F}}{4}\;. \tag{5.2}$$

The coupling to the vector current is

$$S_B = \sum\!\!\!\!\!\!\int_{\{P,R\},K} \bar{\psi}(P)\biggl[\not{B}(K) - \frac{m_\infty^2}{2}\int_v \frac{(i\gamma_0 + \mathbf{v}\cdot\boldsymbol{\gamma})(iB_0 + \mathbf{v}\cdot\mathbf{B})(K)}{(ip_n + \mathbf{v}\cdot\mathbf{p})(ir_n + \mathbf{v}\cdot\mathbf{r})}\biggr]\psi(R)\,\tilde{\delta}(K - P + R)\;. \tag{5.3}$$

It might be expected that the correction here is suppressed by $\mathcal{O}(m_\infty^2/p_n^2) \sim \mathcal{O}(\alpha_{\rm s})$, but this is not the case, because parts of the velocity integral give terms of $\mathcal{O}(m_\infty^2/P^2) \sim \mathcal{O}(1)$.

Let us define an "on-shell" spinor u satisfying

$$\biggl[\not{P} + \frac{m_\infty^2}{2}\int_v \frac{i\gamma_0 + \mathbf{v}\cdot\boldsymbol{\gamma}}{ip_n + \mathbf{v}\cdot\mathbf{p}}\biggr]u(P) = 0\;. \tag{5.4}$$

Consider the dispersion relation following from eq. (5.4). It is known that in Minkowskian space-time the dispersion relation of the "particle branch" reads $p^0 = p + m_\infty^2/(2p) + \ldots$, where $p = |\mathbf{p}|$ [23]. Continuing the frequency to imaginary time, this corresponds to $p_n^2 + p_3^2 + \mathbf{p}_\perp^2 = -m_\infty^2$. Solving for p_3 with a fixed p_n yields

$$\pm ip_3 = p_n + \frac{m_\infty^2}{2p_n} + \frac{\mathbf{p}_\perp^2}{2p_n} + \ldots\;. \tag{5.5}$$

From here a "rest mass" can be identified and subsequently used as a matching coefficient,

$$M_n \equiv p_n + \frac{m_\infty^2}{2p_n} + \mathcal{O}(\alpha_{\rm s}^2 T)\;. \tag{5.6}$$

This agrees with the effective mass derived from an explicit matching computation in ref. [12]; a derivation through HTL expressions like above was previously presented in ref. [24].

The computation of the vertex correction is more cumbersome; however, the task can be simplified by carrying out the matching with the special kinematics[3] $R = -P = -K/2$, in an "on-shell" configuration. Consider the matrix element

$$\Gamma(B) \;\equiv\; \bar{u}(P)\biggl[\not{B}(K) + \frac{m_\infty^2}{2}\int_v \frac{(i\gamma_0 + \mathbf{v}\cdot\boldsymbol{\gamma})(iB_0 + \mathbf{v}\cdot\mathbf{B})(K)}{(ip_n + \mathbf{v}\cdot\mathbf{p})^2}\biggr]u(-P)\;, \quad K = 2P\;. \tag{5.7}$$

[2] In this section spatial vectors are three-dimensional and latin indices run from 1 to 3.

[3] This trick can only be used if $k_n/2$ is an odd multiple of πT, however we assume the result to be general.

JHEP05(2014)117

The velocity integrals appearing here are all doable. In particular, it can be shown that the transverse part of the current, i.e. the part coupling to $\mathbf{B}_T$ with $\mathbf{p}_\perp \cdot \mathbf{B}_T = 0$, has a coefficient $\mathcal{O}(m_\infty^2/p_3^2) \sim \mathcal{O}(\alpha_{\rm s})$; this correction will be neglected in the following.

As far as the longitudinal parts are concerned, we focus on the component coupling to B_0 like before (cf. eq. (2.5)). An explicit computation yields

$$B_0 \int_v \frac{i\gamma_0 + \mathbf{v}\cdot\boldsymbol{\gamma}}{(ip_n + \mathbf{v}\cdot\mathbf{p})^2} = -\frac{B_0}{P^2}\biggl(i\gamma_0 - \frac{ip_n \mathbf{p}\cdot\boldsymbol{\gamma}}{\mathbf{p}^2}\biggr) + \mathcal{O}\Bigl(\frac{1}{\mathbf{p}^2}\Bigr)\,. \tag{5.8}$$

Inserting $P^2 = -m_\infty^2$ and $|\mathbf{p}_\perp| \ll |p_3| \sim |p_n|$ we get a correction of $\mathcal{O}(1)$, so that eq. (5.7) becomes

$$\Gamma(B_0) = B_0\,\bar{u}(P)\biggl[\frac{1}{2}\biggl(\gamma_0 + \frac{p_n}{p_3}\gamma_3\biggr)\biggr]u(-P) + \mathcal{O}(\alpha_{\rm s})\,. \tag{5.9}$$

Rewriting this with 2-component spinors like in eq. (4.8), the HTL-corrected vertex for the operator to which B_0 couples reads

$$S_{B_0} \stackrel{p_n = k_n/2}{\to} \int_{\mathbf{x},z} B_0^{(k_n)}\biggl(\frac{p_3 + ip_n}{2p_3}\chi^\dagger_{p_n}\chi_{-p_n} + \frac{p_3 - ip_n}{2p_3}\phi^\dagger_{p_n}\phi_{-p_n}\biggr) + \mathcal{O}(\alpha_{\rm s})\,. \tag{5.10}$$

However, for the on-shell configuration of $\phi^\dagger_{p_n}$, $p_3 = -ip_n + \mathcal{O}(\alpha_{\rm s})$ (cf. eq. (4.7)). Similarly, for on-shell $\chi^\dagger_{p_n}$, $p_3 = ip_n + \mathcal{O}(\alpha_{\rm s})$. Therefore the prefactors of the operators in eq. (5.10) equal unity. Thus the end result is that for the zero component of the current, we can simply use naive vertices as read off from eq. (4.8).[4]

The non-zero Matsubara modes also induce higher-dimensional operators. In particular, as pointed out in ref. [20], they generate 4-quark operators which can be represented as

$$\delta S_0 = \frac{g^2 T}{2}\sum_{\{p_n,q_n\},\omega_n\neq 0}\frac{1}{\omega_n^2}\int_{\mathbf{x},z}\bigl(\chi^\dagger_{p_n}\,\phi^\dagger_{p_n}\bigr)\,\gamma_0\gamma_\mu\,T^a\begin{pmatrix}\chi_{p_n-\omega_n}\\ \phi_{p_n-\omega_n}\end{pmatrix}\bigl(\chi^\dagger_{q_n}\,\phi^\dagger_{q_n}\bigr)\,\gamma_0\gamma_\mu\,T^a\begin{pmatrix}\chi_{q_n+\omega_n}\\ \phi_{q_n+\omega_n}\end{pmatrix}. \tag{5.11}$$

Here the matrices $\gamma_0\gamma_\mu$ are as given in eq. (2.7), and T^a are Hermitean generators of SU(3), normalized as $\mathrm{Tr}\,[T^a T^b] = \delta_{ab}/2$. The role of these operators is that they cause mixings; for instance, a state $\sim \phi^\dagger_{p_n-\omega_n}\phi_{q_n}$ can be transferred to $\sim \phi^\dagger_{p_n}\phi_{q_n+\omega_n}$, both of which have the same screening mass $p_n - q_n - \omega_n$ at tree level, but a different "decomposition". This implies that all decompositions decay with the same screening mass when δS_0 is included.

6 Schrödinger equation

In this section we recall how the computation of the spatial correlators within the effective theory of sections 4, 5 reduces to the solution of a two-dimensional Schrödinger equation. In particular, we show that in the free limit eqs. (3.12), (3.13), (3.16), (3.17) can be reproduced this way; and that, going to NLO, the equation to be solved is closely related to that for soft-dilepton and photon production in ref. [11]. The theory is the same as in eq. (4.10), with the modification $p_n \to M_n$ as discussed around eq. (5.6).

[4] It can be shown that in the static sector, $k_n = 0$, all vertex corrections are suppressed by $\mathcal{O}(\alpha_{\rm s})$, so that naive vertices again suffice.

JHEP05(2014)117

6.1 Charge density correlator (G_{00})

The charge density can be expressed in terms of low-energy fields as (cf. eqs. (4.4), (4.8))

$$V_0^{(k_n)} = \sum_{0<p_n<k_n} \Big(\chi^\dagger_{p_n} \chi_{p_n-k_n} + \phi^\dagger_{p_n} \phi_{p_n-k_n} \Big) \,. \tag{6.1}$$

The fields $\phi^\dagger_{p_n}$ and $\phi_{p_n-k_n} = \phi_{-|k_n-p_n|}$ are forward-propagating and contribute in eq. (4.1) if $z > 0$. We now rewrite eq. (4.1) with an auxiliary point-splitting in the operator:

$$G_{00}^{(k_n)}(z) = \lim_{\mathbf{y},\mathbf{y}'\to\mathbf{0}} T \int_{\mathbf{x}} \Big\langle V_0^{(k_n)}(\mathbf{x},z;\mathbf{y}) V_0^{(-k_n)}(0;-\mathbf{y}') \Big\rangle_{\rm c} \,, \tag{6.2}$$

where (for $z > 0$)

$$V_0^{(k_n)}(\mathbf{x},z;\mathbf{y}) \;\equiv\; \sum_{0<p_n<k_n} \phi^\dagger_{p_n}\Big(\mathbf{x}+\frac{\mathbf{y}}{2},z\Big)\, W_{\mathbf{y},z}\, \phi_{p_n-k_n}\Big(\mathbf{x}-\frac{\mathbf{y}}{2},z\Big) \,, \tag{6.3}$$

and $W_{\mathbf{y},z}$ is a transverse Wilson line. Computing the correlator to leading order in the weak-coupling expansion and taking already the limit $\mathbf{y}' \to \mathbf{0}$, a straightforward analysis yields

$$G_{00}^{(k_n)}(z) = -\sum_{0<p_n<k_n} 2N_{\rm c} T \lim_{\mathbf{y}\to\mathbf{0}} w_{\rm LO}(z,\mathbf{y}) + \mathcal{O}(\alpha_{\rm s}) \,, \tag{6.4}$$

where

$$w_{\rm LO}(z,\mathbf{y}) \equiv \int_{\mathbf{q}} e^{-i\mathbf{q}\cdot\mathbf{y} - (M_{\rm cm} + \frac{q^2}{2M_{\rm r}})|z|} \,. \tag{6.5}$$

Here

$$M_{\rm cm} \equiv k_n + \frac{m_\infty^2}{2M_{\rm r}} \,, \quad M_{\rm r} \equiv \biggl(\frac{1}{p_n} + \frac{1}{k_n - p_n} \biggr)^{-1} \,. \tag{6.6}$$

Two things can be learned from eq. (6.5). First, $w_{\rm LO}$ can equivalently be represented as a solution of a first order differential equation with a particular boundary condition,

$$\Big(\partial_z + M_{\rm cm} - \frac{\nabla^2}{2M_{\rm r}} \Big) w_{\rm LO}(z,\mathbf{y}) = 0 \,, \quad z > 0 \,, \tag{6.7}$$

$$w_{\rm LO}(0,\mathbf{y}) = \delta^{(2)}(\mathbf{y}) \,. \tag{6.8}$$

Second, the point-split spectral function corresponding to eq. (6.5) can be determined,

$$\rho_{\rm LO}(\omega,\mathbf{y}) = \int_{\mathbf{q}} e^{-i\mathbf{q}\cdot\mathbf{y}}\, \pi\delta\Big(\omega - M_{\rm cm} - \frac{q^2}{2M_{\rm r}} \Big) \,, \quad \omega > 0 \,. \tag{6.9}$$

The original spectral function thereby becomes, combining eqs. (6.4) and (6.9),

$$\rho_{00}^{(k_n)}(\omega) \;=\; -\sum_{0<p_n<k_n} 2N_{\rm c} T \lim_{\mathbf{y}\to\mathbf{0}} \rho_{\rm LO}(\omega,\mathbf{y}) \;=\; -\sum_{0<p_n<k_n} N_{\rm c} T M_{\rm r}\, \theta\big(\omega - M_{\rm cm}\big) \,. \tag{6.10}$$

Setting $n = 1$ and considering the leading order (i.e. $m_\infty^2 \to 0$), we have $M_{\rm cm} = k_1$ and $M_{\rm r} = k_1/4$. Then eq. (6.10) agrees with eq. (3.12) when the latter is expanded to leading non-trivial order in $\omega - k_1$ (the case of general k_n is discussed in appendix A).

JHEP05(2014)117

Consider now NLO corrections to eq. (6.2). Keeping $\mathbf{y},\mathbf{y}'\neq\mathbf{0}$, the computation can be carried out by omitting the transverse motion suppressed by $1/(2M_{\rm r})$, whereby the quark propagators are straight Wilson lines. Sending $z\to\infty$ and suppressing $\mathbf{y}'$, we obtain

$$\big(\partial_z + M_{\rm cm}\big) w_{\rm NLO}(z,\mathbf{y}) \stackrel{z\to\infty}{=} -V^+_{\rm LO}(\mathbf{y}) w_{\rm LO}(z,\mathbf{y})\,, \tag{6.11}$$

$$\begin{aligned} V^+_{\rm LO}(\mathbf{y}) &\equiv g_{\rm E}^2 C_{\rm F} \int_{\mathbf{q}} \Big(1-e^{i\mathbf{q}\cdot\mathbf{y}}\Big)\bigg(\frac{1}{\mathbf{q}^2}-\frac{1}{\mathbf{q}^2+m_{\rm E}^2}\bigg) \\ &= \frac{g_{\rm E}^2 C_{\rm F}}{2\pi}\bigg[\ln\Big(\frac{m_{\rm E} y}{2}\Big)+\gamma_{\rm E}+K_0(m_{\rm E} y)\bigg]\,, \end{aligned} \tag{6.12}$$

where $C_F=(N_{\rm c}^2-1)/(2N_{\rm c})$; $g_{\rm E}^2=g^2T$ is the gauge coupling of the dimensionally reduced theory; $m_{\rm E}^2=(\frac{N_{\rm c}}{3}+\frac{N_{\rm f}}{6})g^2T^2$ is the Debye mass parameter appearing in the static propagator of A_0; and K_0 is a modified Bessel function.

We finally combine eqs. (6.7), (6.11). If we set $w_{\rm LO}\sim\mathcal{O}(1)$, than according to eq. (6.11), $w_{\rm NLO}\sim\mathcal{O}(\alpha_{\rm s})$. Moreover, in the kinematic regime $\nabla\sim gT$ of relevance to us, $-\nabla^2/M_{\rm r}\sim\mathcal{O}(\alpha_{\rm s})$. It follows that, up to a perturbative error of $\sim\mathcal{O}(\alpha_{\rm s}^2)$, we can write

$$(\partial_z+\hat{H}^+)w(z,\mathbf{y})=0\,,\quad z>0\,, \tag{6.13}$$

where $w=w_{\rm LO}+w_{\rm NLO}+\ldots$ and we have denoted

$$\hat{H}^+\equiv M_{\rm cm}-\frac{\nabla^2}{2M_{\rm r}}+V^+\,. \tag{6.14}$$

The initial condition remains that same as in eq. (6.8), up to corrections of $\mathcal{O}(\alpha_{\rm s})$.

The Schrödinger equation and the initial condition can be combined into a single equation by taking a Fourier transform. The system

$$\partial_z w(z,\mathbf{y}) = -\mathrm{sign}(z)\,\hat{H}^+\,w(z,\mathbf{y})\,,\quad w(0,\mathbf{y})=\delta^{(2)}(\mathbf{y}) \tag{6.15}$$

can formally be solved as $w(z,\mathbf{y})=e^{-\hat{H}^+|z|}w(0,\mathbf{y})$. Its Fourier transform (cf. eq. (2.2)) reads

$$w(k_3,\mathbf{y})=\Big([ik_3+\hat{H}^+]^{-1}-[ik_3-\hat{H}^+]^{-1}\Big)\delta^{(2)}(\mathbf{y})\,. \tag{6.16}$$

The spectral function follows from the cut. Defining an auxiliary function $g(\omega,\mathbf{y})$ as the solution of a z-independent inhomogeneous equation

$$\Big(\hat{H}^+-\omega-i0^+\Big)g^+(\omega,\mathbf{y})=\delta^{(2)}(\mathbf{y})\,, \tag{6.17}$$

we obtain (for $\omega>0$ and assuming a positive spectrum)

$$\rho_{00}^{(k_n)}(\omega)=-\sum_{0<p_n<k_n} 2N_{\rm c}T\lim_{\mathbf{y}\to\mathbf{0}}\mathrm{Im}\,g^+(\omega,\mathbf{y})\,. \tag{6.18}$$

It may be noted that eqs. (6.17), (6.18) bear a close resemblance to the corresponding equations appearing in the LPM resummation of longitudinal modes for dilepton production, cf. eqs. (22), (24) of ref. [11]. The overall normalizations of g^+, as determined by the coefficient of the inhomogeneous term, as well as of the parameters appearing do differ, but

JHEP05(2014)117

this is a matter of conventions. In addition some imaginary parts appear differently,[5] but this is related to the Minkowskian versus Euclidean nature of the observable considered. The functional form of the potential appearing in $\hat{H}^+$ is identical, as well as the fact that we are looking for a scalar (S-wave) solution, as determined by the inhomogeneous term.

6.2 Transverse current correlator (G_T)

Let us repeat the analysis for the transverse components of the current, cf. eq. (2.6). We again introduce an auxiliary point-splitting into the currents:

$$G_T^{(k_n)}(z) = \lim_{\mathbf{y},\mathbf{y}'\to\mathbf{0}} T\sum_{i=1}^{2}\int_{\mathbf{x}}\Big\langle V_i^{(k_n)}(\mathbf{x},z;\mathbf{y})V_i^{(-k_n)}(0;-\mathbf{y}')\Big\rangle_{\mathrm{c}}\,, \tag{6.19}$$

where, following eq. (4.11),

$$V_i^{(k_n)}(\mathbf{x},z;\mathbf{y}) \equiv \sum_{0<p_n<k_n} \tag{6.20}$$
$$\phi^\dagger_{p_n}\Big(\mathbf{x}+\frac{\mathbf{y}}{2}\,,z\Big)\bigg\{\Big(\frac{1}{p_n}-\frac{1}{k_n-p_n}\Big)\frac{\overleftrightarrow{D}_i}{4i}-\Big(\frac{1}{p_n}+\frac{1}{k_n-p_n}\Big)\frac{\sigma_3\epsilon_{ij}\overleftrightarrow{D}_j}{4}\bigg\}\phi_{p_n-k_n}\Big(\mathbf{x}-\frac{\mathbf{y}}{2}\,,z\Big)\,,$$

with the notation $\overleftrightarrow{D}_j \equiv W_{\mathbf{y},z}\overrightarrow{D}_j - \overleftarrow{D}_j W_{\mathbf{y},z}$. At leading order,

$$G_T^{(k_n)}(z) = -\sum_{0<p_n<k_n} N_{\mathrm{c}}T\bigg[\frac{1}{p_n^2}+\frac{1}{(k_n-p_n)^2}\bigg]\lim_{\mathbf{y}\to\mathbf{0}}\nabla\cdot\mathbf{v}_{\mathrm{LO}}(z,\mathbf{y})+\mathcal{O}(\alpha_{\mathrm{s}})\,, \tag{6.21}$$

where we already took $\mathbf{y}'\to\mathbf{0}$ and defined

$$\mathbf{v}_{\mathrm{LO}}(z,\mathbf{y}) \equiv \int_{\mathbf{q}} i\mathbf{q}\,e^{-i\mathbf{q}\cdot\mathbf{y}-(M_{\mathrm{cm}}+\frac{q^2}{2M_{\mathrm{r}}})|z|}\,. \tag{6.22}$$

Like with the charge density, the LO solution can be represented as a differential equation,

$$\Big(\partial_z + M_{\mathrm{cm}} - \frac{\nabla^2}{2M_{\mathrm{r}}}\Big)\mathbf{v}_{\mathrm{LO}}(z,\mathbf{y}) = 0\,,\quad z>0\,, \tag{6.23}$$
$$\mathbf{v}_{\mathrm{LO}}(0,\mathbf{y}) = -\nabla\delta^{(2)}(\mathbf{y})\,. \tag{6.24}$$

Also, a point-split spectral function corresponding to eq. (6.22) can be determined,

$$\boldsymbol{\rho}_{\mathrm{LO}}(\omega,\mathbf{y}) = \int_{\mathbf{q}} i\mathbf{q}\,e^{-i\mathbf{q}\cdot\mathbf{y}}\,\pi\delta\Big(\omega - M_{\mathrm{cm}} - \frac{q^2}{2M_{\mathrm{r}}}\Big)\,,\quad \omega>0\,. \tag{6.25}$$

The original spectral function thereby becomes (cf. eq. (6.21))

$$\begin{aligned}\rho_{T,\mathrm{LO}}^{(k_n)}(\omega) &= -\sum_{0<p_n<k_n} N_{\mathrm{c}}T\bigg[\frac{1}{p_n^2}+\frac{1}{(k_n-p_n)^2}\bigg]\lim_{\mathbf{y}\to\mathbf{0}}\nabla\cdot\boldsymbol{\rho}_{\mathrm{LO}}(\omega,\mathbf{y})\\ &= -\sum_{0<p_n<k_n} N_{\mathrm{c}}T\bigg[\frac{1}{p_n^2}+\frac{1}{(k_n-p_n)^2}\bigg]M_{\mathrm{r}}^2\big(\omega-M_{\mathrm{cm}}\big)\,\theta\big(\omega-M_{\mathrm{cm}}\big)\,.\end{aligned} \tag{6.26}$$

[5] In particular, in LPM resummation the potential plays the role of a "width".

JHEP05(2014)117

The parameters appearing here are defined in eq. (6.6). For $n = 1$ eq. (6.26) agrees with eq. (3.13) when the latter is expanded to leading non-trivial order in $\omega - k_1$ (the case $n > 1$ is discussed in appendix A).

The inclusion of interactions proceeds like for the charge density, with the only difference that the "wave function" is now a vector. In particular, introducing a z-independent inhomogeneous Schrödinger equation

$$\Big(\hat{H}^+ - \omega - i0^+\Big)\mathbf{f}^+(\omega,\mathbf{y}) = -\nabla\delta^{(2)}(\mathbf{y})\;, \tag{6.27}$$

the cut of the solution (denoted by Im) yields the spectral function, and

$$\rho_T^{(k_n)}(\omega) = -\sum_{0<p_n<k_n} N_{\rm c}T\left[\frac{1}{p_n^2} + \frac{1}{(k_n-p_n)^2}\right]\lim_{\mathbf{y}\to\mathbf{0}}\mathrm{Im}\,\nabla\cdot\mathbf{f}^+(\omega,\mathbf{y})\;. \tag{6.28}$$

Equations (6.27), (6.28) again have the same general form as the ones in the LPM resummation of the photon or dilepton production rate, cf. eqs. (22), (24) of ref. [11], with differences originating from the chosen normalization and parameters and from differences of the signatures. The functional form of the potential is the same, as is the fact that we are looking for a vector-valued (P-wave) solution, as dictated by the inhomogeneous term in eq. (6.27).

6.3 Static sector

The static case $k_n = 0$ differs qualitatively from $k_n \neq 0$. We go here beyond the previous discussion of ref. [12] by including the charge density correlator and by giving the inhomogeneous Schrödinger equations determining the absolute values of the correlators.

Starting with the transverse case (which for $n = 0$ corresponds to the S-wave), we write

$$G_T^{(0)}(z) = \lim_{\mathbf{y},\mathbf{y}'\to\mathbf{0}} T\sum_{i=1}^{2}\int_{\mathbf{x}}\Big\langle V_i^{(0)}(\mathbf{x},z;\mathbf{y})V_i^{(0)}(0;-\mathbf{y}')\Big\rangle_{\rm c}\;, \tag{6.29}$$

where (cf. eq. (4.8))

$$V_i^{(0)}(\mathbf{x},z;\mathbf{y}) \;\equiv\; \sum_{\{p_n\}}\epsilon_{ij}\left[\phi^\dagger_{p_n}\Big(\mathbf{x}+\frac{\mathbf{y}}{2}\,,z\Big)\sigma_j\,W_{\mathbf{y},z}\,\chi_{p_n}\Big(\mathbf{x}-\frac{\mathbf{y}}{2}\,,z\Big) - (\chi\leftrightarrow\phi)\right]. \tag{6.30}$$

The subsequent steps go as in section 6.1, with the difference that the fields appearing are $\phi^\dagger_{p_n}\chi_{p_n}$ rather than $\phi^\dagger_{p_n}\phi_{-p'_n}$, which leads to a different potential [12]:

$$V^-_{\rm LO}(\mathbf{y}) \;\equiv\; g_{\rm E}^2 C_{\rm F}\int_{\mathbf{q}}\left(\frac{1-e^{i\mathbf{q}\cdot\mathbf{y}}}{\mathbf{q}^2} - \frac{1+e^{i\mathbf{q}\cdot\mathbf{y}}}{\mathbf{q}^2+m_{\rm E}^2}\right) \;=\; \frac{g_{\rm E}^2 C_{\rm F}}{2\pi}\left[\ln\Big(\frac{m_{\rm E}y}{2}\Big)+\gamma_{\rm E}-K_0(m_{\rm E}y)\right]. \tag{6.31}$$

With this potential the Hamiltonian reads

$$\hat{H}^- \equiv M_{\rm cm} - \frac{\nabla^2}{2M_{\rm r}} + V^-\;,\quad M_{\rm cm} = 2p_n + \frac{m_\infty^2}{2M_{\rm r}}\;,\quad M_{\rm r} = \frac{p_n}{2}\;. \tag{6.32}$$

The inhomogeneous Schrödinger equation becomes

$$\Big(\hat{H}^- - \omega - i0^+\Big)g^-(\omega,\mathbf{y}) = \delta^{(2)}(\mathbf{y})\;, \tag{6.33}$$

JHEP05(2014)117

and the spectral function is

$$\rho_T^{(0)}(\omega) = -\sum_{p_n>0} 8N_c T \lim_{\mathbf{y}\to\mathbf{0}} \mathrm{Im}\, g^-(\omega,\mathbf{y})\,. \tag{6.34}$$

Here the modes $p_n > 0$ and $p_n < 0$ have been summed together even though, when 4-quark operators are included, their degeneracy may be lifted. In the free limit the result can be extracted from eq. (6.10), and agrees with the threshold expansion of eq. (3.17).

The charge density correlator (which for $n = 0$ corresponds to the P-wave) reads

$$G_{00}^{(0)}(z) = \lim_{\mathbf{y},\mathbf{y}'\to\mathbf{0}} T\int_{\mathbf{x}} \Big\langle V_0^{(0)}(\mathbf{x},z;\mathbf{y}) V_0^{(0)}(0;-\mathbf{y}')\Big\rangle_{\mathrm{c}}\,, \tag{6.35}$$

where from eq. (4.12),

$$V_0^{(0)}(\mathbf{x},z;\mathbf{y}) \;\equiv\; \sum_{\{p_n\}} \frac{\epsilon_{ij}}{2ip_n}\left[\phi^\dagger_{p_n}\Big(\mathbf{x}+\frac{\mathbf{y}}{2}\,,z\Big)\sigma_i \overleftrightarrow{D}_j \chi_{p_n}\Big(\mathbf{x}-\frac{\mathbf{y}}{2}\,,z\Big) - (\chi\leftrightarrow\phi)\right]. \tag{6.36}$$

The inhomogeneous Schrödinger equation reads

$$\Big(\hat{H}^- - \omega - i0^+\Big)\mathbf{f}^-(\omega,\mathbf{y}) = -\nabla\delta^{(2)}(\mathbf{y})\,, \tag{6.37}$$

and the spectral function is

$$\rho_{00}^{(0)}(\omega) = -\sum_{p_n>0}\frac{4N_c T}{p_n^2}\lim_{\mathbf{y}\to\mathbf{0}}\mathrm{Im}\,\nabla\cdot\mathbf{f}^-(\omega,\mathbf{y})\,. \tag{6.38}$$

Again the modes $p_n > 0$ and $p_n < 0$ have been summed together. In the free limit, the result can be extracted from eq. (6.26), and agrees with the threshold expansion of eq. (3.16).

7 Non-perturbative potential and numerical predictions

The potential given in eq. (6.12) can be defined more generally from point-split correlators such as eq. (6.2). It can be defined in the "infinite-mass" limit ($\nabla^2/M_{\mathrm{r}} \ll M_{\mathrm{cm}}$), whereby the propagators are just straight lines. In this situation we can set $\mathbf{y}' = \mathbf{y}$ and $\mathbf{x} = \mathbf{0}$ in eq. (6.2). More specifically, let us define a loop ($z > 0$)

$$\begin{aligned} L(\mathbf{y},z) &\equiv \lim_{M_{\mathrm{cm}}\to\infty} e^{M_{\mathrm{cm}}z}\Big\langle V_0^{(k_n;p_n)}(\mathbf{0},z;\mathbf{y})\, V_0^{(-k_n;-q_n)}(0;-\mathbf{y})\Big\rangle \\ &= -\mathrm{Tr}\,\Big\langle U_2^\dagger\Big(\frac{\mathbf{y}}{2}\,,z\Big)\, W_{\mathbf{y},z}\, U_1\Big(-\frac{\mathbf{y}}{2}\,,z\Big)\, W^\dagger_{\mathbf{y},0}\Big\rangle\,, \end{aligned} \tag{7.1}$$

where we inserted eq. (6.3), restricted to a contribution from a single p_n, and defined the "longitudinal" Wilson lines as ($q_n \equiv k_n - p_n$)

$$U_1\Big(-\frac{\mathbf{y}}{2}\,,z\Big) \equiv \lim_{M_{q_n}\to\infty} e^{M_{q_n}z}\Big\langle\phi_{-q_n}\Big(-\frac{\mathbf{y}}{2}\,,z\Big)\phi^\dagger_{-q_n}\Big(-\frac{\mathbf{y}}{2}\,,0\Big)\Big\rangle_A\,, \tag{7.2}$$

$$U_2^\dagger\Big(\frac{\mathbf{y}}{2}\,,z\Big) \equiv \lim_{M_{p_n}\to\infty} e^{M_{p_n}z}\Big\langle\phi_{p_n}\Big(\frac{\mathbf{y}}{2}\,,0\Big)\phi^\dagger_{p_n}\Big(\frac{\mathbf{y}}{2}\,,z\Big)\Big\rangle_A\,. \tag{7.3}$$

JHEP05(2014)117

Here $\langle \ldots \rangle_A$ denotes a fermion propagator in a fixed gauge field background. The Wilson lines satisfy the equations of motion

$$\partial_z U_1\Big(-\frac{\mathbf{y}}{2},z\Big) = \big(igA_3 - gA_0\big)\, U_1\Big(-\frac{\mathbf{y}}{2},z\Big)\;, \tag{7.4}$$

$$\partial_z U_2^\dagger\Big(\frac{\mathbf{y}}{2},z\Big) = U_2^\dagger\Big(\frac{\mathbf{y}}{2},z\Big)\big(-igA_3 + gA_0\big)\;, \tag{7.5}$$

which can be integrated in terms of path-ordered exponentials as usual. Note that $L(\mathbf{y},z)$ is z-independent at $\mathbf{y}=\mathbf{0}$. The potential is subsequently extracted from

$$V^+(\mathbf{y}) \equiv -\lim_{z\to\infty} L^{-1}(\mathbf{y},z)\partial_z L(\mathbf{y},z)\;. \tag{7.6}$$

This potential vanishes for $\mathbf{y}=\mathbf{0}$. The choice of the transverse Wilson lines $W, W^\dagger$ affects the overall value of L but not that of the exponential falloff, which can be viewed as an eigenvalue of a Hamiltonian.

The potential of eq. (7.6) agrees with the one derived and computed up to $\mathcal{O}(\alpha_{\rm s}^{3/2})$ in ref. [9]. A coordinate space expression was given in ref. [25]. The potential has been measured within a dimensionally reduced effective field theory (EQCD) in ref. [10]; we make use of the "cold" ($T\approx 400\,\mathrm{MeV}$) $\beta=16$ data set.[6] At short distances, a polynomial interpolation is employed; for estimating the potential at distances larger than those for which measurements exist, we fit the 5 largest distances ($yg_{\rm E}^2>2.5$) to the confining form $\sigma y+\mu+\frac{\gamma}{y}$ which describes the asymptotics well [27].[7]

We express the screening masses as "energies",

$$E_{\rm full} = M_{\rm cm} + \frac{g_{\rm E}^2 C_{\rm F}}{2\pi}\hat{E}\;, \tag{7.7}$$

and define the dimensionless quantities

$$\bar{y} \equiv m_{\rm E} y\;, \quad \rho \equiv \frac{g_{\rm E}^2 C_{\rm F} M_{\rm r}}{\pi m_{\rm E}^2}\;, \tag{7.8}$$

where $M_{\rm r}$ is the reduced mass (cf. eqs. (6.6), (6.32)). The radial homogeneous part of the Schrödinger equation to be solved (cf. eqs. (6.17), (6.27), (6.33), (6.37)) reads

$$\bigg\{-\frac{\mathrm{d}^2}{\mathrm{d}\bar{y}^2} - \frac{1}{\bar{y}}\frac{\mathrm{d}}{\mathrm{d}\bar{y}} + \frac{l^2}{\bar{y}^2} + \rho\bigg(\frac{2\pi V^\pm}{g_{\rm E}^2 C_{\rm F}} - \hat{E}^{(l)}\bigg)\bigg\} R_l = 0\;, \tag{7.9}$$

where $l=0,1,2,\ldots$ denotes the angular quantum number. Assuming R_l finite at $\bar{y}=0$ and integrable at $\bar{y}\to\infty$, the eigenvalues $\hat{E}^{(l)}$ are easily determined numerically. Results for the ground state ($\hat{E}_0^{(l)}$) for V^+ are shown in figure 2(left) and for V^- in figure 3(left).

Apart from the energies, the magnitudes of the correlators are also of interest. These can be obtained by solving eqs. (6.17), (6.27) in a spectral representation. Assuming a

[6] At present no continuum extrapolation exists, but the necessary ingredients have been discussed [26].

[7] However at very large y, when the value of V^+ exceeds $2\pi T$, we should expect string breaking to set in.

JHEP05(2014)117

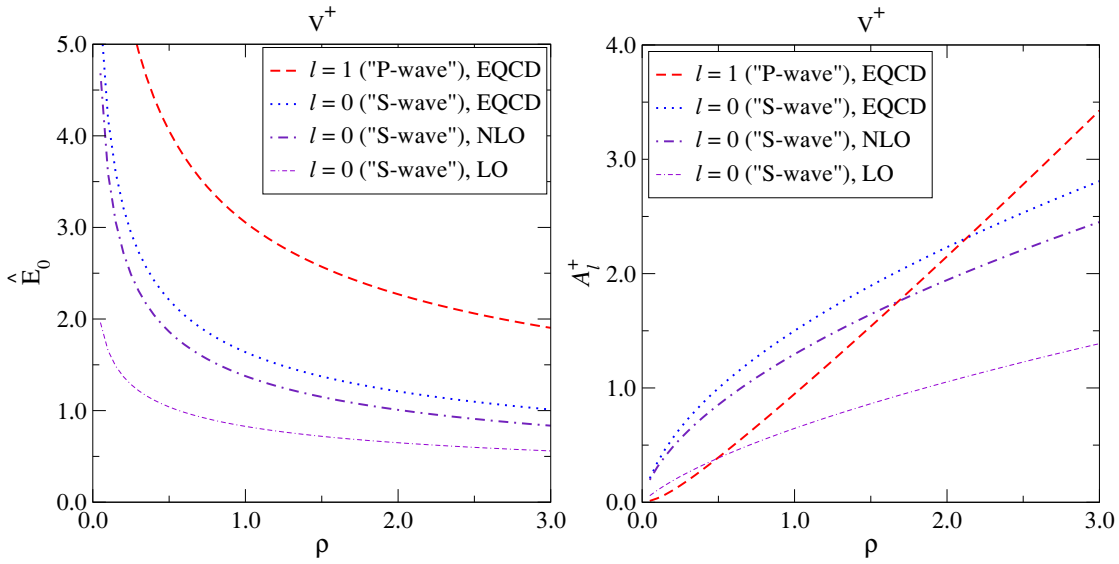

Figure 2. Left: the lowest "S-wave" eigenvalue obtained with the LO (eq. (6.12)), NLO [9], and EQCD potential V^+ [10]. For EQCD the "P-wave" result is shown as well. For the LO case the leading-log asymptotics read $\hat{E}_0 \approx \frac{1}{2}\ln\frac{1}{\rho}$ for $\rho \ll 1$ and $\hat{E}_0 \approx (\frac{\ln\rho}{2\rho})^{\frac{1}{2}}$ for $\rho \gg 1$. Right: the "amplitudes" corresponding to the lowest eigenmodes, as defined in the text (cf. eqs. (7.11), (7.14)).

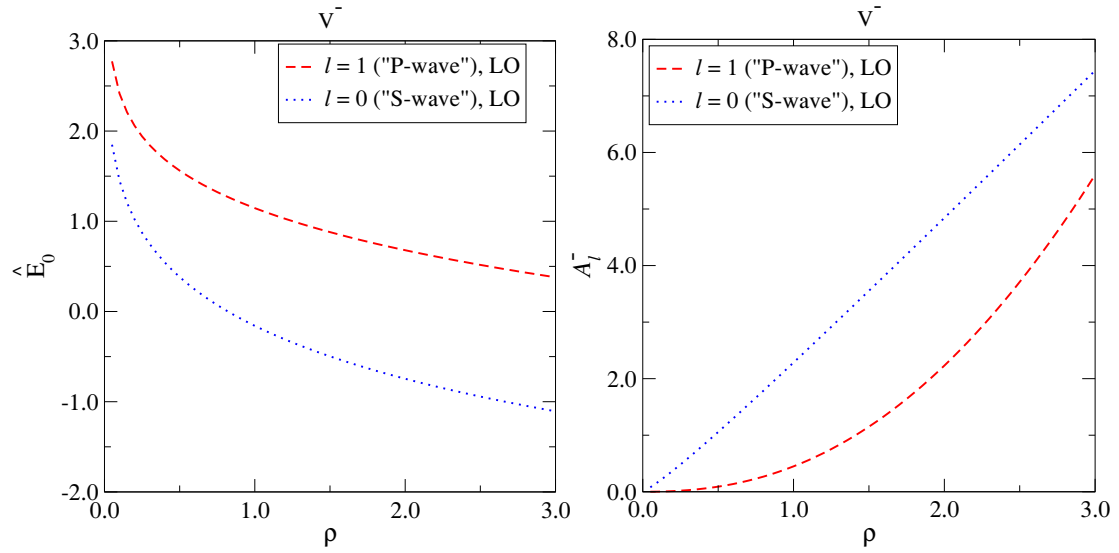

Figure 3. Left: the lowest "S-wave" and "P-wave" eigenvalues obtained with the LO potential $V^-_{\rm LO}$ (cf. eq. (6.31)). Right: the "amplitudes" corresponding to the lowest eigenmodes (cf. eq. (7.15)).

discrete spectrum and letting ψ_i be wave functions normalized as $\int \mathrm{d}^2\mathbf{y}\,\psi_i^*(\mathbf{y})\psi_j(\mathbf{y}) = \delta_{ij}$, the solution of eq. (6.17) and subsequently (6.18) reads

$$g^+(\omega,\mathbf{y}) = \sum_{i=0}^{\infty} \frac{\psi_i(\mathbf{y})\psi_i^*(\mathbf{0})}{E_i - \omega - i0^+}\,, \quad \rho_{00}^{(k_n)}(\omega) = -2\pi N_{\rm c} T \sum_{i=0}^{\infty} \delta(E_i-\omega)|\psi_i(\mathbf{0})|^2\,, \tag{7.10}$$

JHEP05(2014)117

where the sum $\sum_{0<p_n<k_n}$ has been suppressed for notational simplicity. Inserting this into eq. (2.4), we obtain the long-distance asymptotics

$$-\frac{G_{00}^{(k_n)}(z)}{T^3} \approx \frac{N_{\rm c} m_{\rm E}^2\, \mathcal{A}_0^+}{\pi T^2}\, e^{-|z|E_0^{(l=0)}} \,, \quad \mathcal{A}_0^+ \equiv \frac{|R_0(0)|^2}{\int_0^\infty {\rm d}\bar{y}\, \bar{y}\, |R_0(\bar{y})|^2} \,. \tag{7.11}$$

For the P-wave case, eqs. (6.27), (6.28) lead similarly to

$$\mathbf{f}^+(\omega,\mathbf{y}) = \sum_{i=0}^{\infty} \frac{\psi_i(\mathbf{y}) \nabla \psi_i^*(\mathbf{0})}{E_i - \omega - i0^+} \,, \tag{7.12}$$

$$\rho_T^{(k_n)}(\omega) = -\pi N_{\rm c} T \biggl[\frac{1}{p_n^2} + \frac{1}{(k_n-p_n)^2}\biggr] \sum_{i=0}^{\infty} \delta(E_i-\omega) |\nabla\psi_i(\mathbf{0})|^2 \,, \tag{7.13}$$

and the configuration space correlator reads (for $|z| \gg 1/[E_1^{(l=1)} - E_0^{(l=1)}]$)

$$-\frac{G_T^{(k_n)}(z)}{T^3} \approx \frac{N_{\rm c} m_{\rm E}^4\, \mathcal{A}_1^+}{\pi T^2} \biggl[\frac{1}{p_n^2} + \frac{1}{(k_n-p_n)^2}\biggr] e^{-|z|E_0^{(l=1)}} \,, \quad \mathcal{A}_1^+ \equiv \frac{|R_1'(0)|^2}{\int_0^\infty {\rm d}\bar{y}\, \bar{y}\, |R_1(\bar{y})|^2} \,. \tag{7.14}$$

The "amplitudes" $\mathcal{A}_0^+, \mathcal{A}_1^+$ are illustrated for the various potentials in figure 2(right).

In the static sector, we similarly get from eqs. (6.34) and (6.38)

$$-\frac{G_T^{(0)}(z)}{T^3} \approx \frac{4N_{\rm c} m_{\rm E}^2\, \mathcal{A}_0^-}{\pi T^2}\, e^{-|z|E_0^{(l=0)}} \,, \quad -\frac{G_{00}^{(0)}(z)}{T^3} \approx \frac{4N_{\rm c} m_{\rm E}^4\, \mathcal{A}_1^-}{\pi T^2 p_n^2}\, e^{-|z|E_0^{(l=1)}} \,, \tag{7.15}$$

where the eigenvalues and eigenfunctions are solved with $\hat{H}^-$, and the suppressed sum now reads $\sum_{p_n>0}$. The "amplitudes" $\mathcal{A}_0^-, \mathcal{A}_1^-$ are illustrated in figure 3(right).

There is one more comment to make about the energies in eq. (7.7). For the non-static case, eq. (6.6) implies

$$E_0^{(l)} = M_{\rm cm} + \frac{g_{\rm E}^2 C_{\rm F}}{2\pi} \hat{E}_0^{(l)} = k_n + \frac{g_{\rm E}^2 C_{\rm F}}{2\pi} \biggl[\frac{\pi T}{4M_{\rm r}} + \hat{E}_0^{(l)}\biggr] \,. \tag{7.16}$$

Here we have re-expressed the parameter m_∞^2 of eq. (5.2) in terms of the gauge coupling $g_{\rm E}^2$. It should be noted however that m_∞^2 is only known at 1-loop level whereas the parameters $m_{\rm E}^2$ and $g_{\rm E}^2$ are known at 2-loop level. Within the same approximation, the ground state energies of the static sector are of the form

$$E_0^{(l)} = k_1 + \frac{g_{\rm E}^2 C_{\rm F}}{2\pi} \biggl[\frac{1}{2} + \hat{E}_0^{(l)}\biggr] \,. \tag{7.17}$$

8 Lattice simulations

8.1 Basic setup

For a non-perturbative crosscheck we make use of lattice simulations in two-flavour QCD, with physical parameters corresponding to $\Lambda_{\overline{\rm MS}} = 310(20)\,{\rm MeV}$ and $m_\pi \approx 270\,{\rm MeV}$ [28]. Lattices of spatial size $N_s^3 = 64^3$ and lattice spacing $a = 0.0486(4)(5)\,{\rm fm}$ are considered.

JHEP05(2014)117

$T/\Lambda_{\overline{\rm MS}}$	$g_{\rm E}^2/T$	$m_{\rm E}^2/T^2$	$\rho^{(n=0,1)}$	$\rho^{(n=2)}$
0.82(5)	3.2(2)	3.5(4)	0.61(4)	0.92(9)
1.09(7)	2.8(2)	3.1(3)	0.61(2)	0.91(4)

Table 1. The effective gauge coupling, mass parameter, and ρ-parameter (cf. eq. (7.8)) for the different sectors, according to the 2-loop computations in refs. [30, 31]. The two temperatures correspond to $T = 254(4)\,\mathrm{MeV}$ and $T = 338(5)\,\mathrm{MeV}$, respectively, for $N_{\rm f} = 2$ QCD. The errors are based on variations of the renormalization scale.

	$T/\Lambda_{\overline{\rm MS}} = 0.82(5)$			$T/\Lambda_{\overline{\rm MS}} = 1.09(7)$		
	$n=0$	$n=1$	$n=2$	$n=0$	$n=1$	$n=2$
degeneracy	2	1	2	2	1	2
E_{00}/T	7.6(1)*	8.0(2)	14.0(1)	7.5(1)*	7.8(1)	13.8(1)
E_T/T	6.8(1)*	9.2(2)	15.0(2)	6.7(1)*	8.9(2)	14.7(1)
A_{00}/T^3	0.7(2)*	3.8(5)	9.6(12)	0.5(1)*	3.3(3)	8.5(8)
A_T/T^3	17.8(22)*	1.2(4)	2.3(6)	15.7(14)*	1.0(2)	1.8(3)

Table 2. Weak-coupling (for $n = 0$, marked with an asterisk) and EQCD (for $n > 0$) predictions for screening masses and "amplitudes", with the latter defined as $G \equiv -A\, e^{-E|z|}$ at large $|z|$. For the amplitudes all states that are degenerate at the current level of precision have been summed together. The errors, based on those in table 1, should be considered as underestimates.

The thermal ensembles have temporal extents $N_\tau = 16, 12$, corresponding to the temperatures $T = 254(4)\,\mathrm{MeV}$ and $T = 338(5)\,\mathrm{MeV}$, respectively. (In terms of the pseudocritical temperature of the QCD crossover these amount to $T/T_{\rm c} \simeq 1.2$ and $T/T_{\rm c} \simeq 1.6$ at $N_{\rm f} = 2$ [29].) Further details concerning the lattice setup and measurements are given in appendix B.

For a comparison with the results of the previous sections, the parameters of the effective theory need to be estimated. The 2-loop values for these, as well as for the parameter ρ defined in eq. (7.8), are given in table 1. The subsequent predictions for the four-dimensional physical observables are shown in table 2. The energies come from eqs. (7.16) and (7.17); the amplitudes from eqs. (7.11), (7.14) and (7.15).

To the order we are working at, the ground state is degenerate in several channels (cf. table 2). We expect this degeneracy to be lifted at higher orders, in particular by the effect of the term δS_0 in the action (cf. eq. (5.11)). In the practical lattice analysis we see no indications of closely lying states. Therefore, in the following, only single states are discussed on both sides.

JHEP05(2014)117

	$T/\mathrm{MeV} = 254(4)$			$T/\mathrm{MeV} = 338(5)$		
	$n=0$	$n=1$	$n=2$	$n=0$	$n=1$	$n=2$
E_{00}/T	7.87(10)	7.45(6)	13.6(4)*	7.69(23)	7.252(11)	12.68(12)*
E_{33}/T	—	7.38(5)	12.77(17)*	—	7.16(3)	12.71(24)*
E_T/T	5.76(4)	9.35(20)	—	6.097(12)	9.48(13)	—
A_{00}/T^3	7.9(7)	6.0(4)	23.5(77)*	4.1(16)	4.78(7)	15.8(16)*
A_{33}/T^3	—	4.00(20)	16.7(16)*	—	3.15(18)	15.4(31)*
A_T/T^3	10.3(4)	9.2(16)	—	10.63(13)	10.0(12)	—

Table 3. Lattice results for the screening masses and "amplitudes". The errors are statistical, with no estimate of systematics related to cutoff effects. For $n \neq 0$ the screening masses E_{00} and E_{33} should agree because of a Ward identity. For $n = 0$ the correlator G_{33} is conserved and no screening mass can be extracted. For $n = 2$ the data (marked with an asterisk) is noisy and the distances probed are close to the scale of the lattice spacing, so that systematic uncertainties could be large. We get no signal for the transverse correlator at $n = 2$.

8.2 Fitting strategy

In order to extract the screening masses and amplitudes from the non-perturbative lattice correlators, a fitting ansatz needs to be chosen. The discussion below refers to the form

$$G_{\cosh}(z) \equiv A\,\frac{\cosh[M(z-L_z/2)]}{\sinh[ML_z/2]}\,, \quad L_z \equiv 64a\,, \tag{8.1}$$

but we have also considered purely exponential fits of the form $G_{\exp}(z) \equiv \sum_{n=1}^{2} A_n\, e^{-M_n z}$. The right edge of the fitting range is set to $L_z/2$, and the fits are repeated for all possible positions of the left edge. The results are extracted from uncorrelated fits with errors originating from a jackknife procedure. To decide which of the resulting parameters is the best we impose a stability criterion with respect to the position of the left edge. To this end we compute the adjacent and next-to-adjacent edge-position parameter values and demand that the difference of their average and the current parameters be smaller than some tolerance. In the next step we reduce this tolerance to the point where only a single parameter set fulfills the stability criterion, and quote this number as our final result.

The qualities of such fits can be illustrated by defining "effective masses" and "effective amplitudes". Effective masses are defined by the implicit equation

$$\frac{G(z-a/2)}{G(z+a/2)} = \frac{\cosh\left[M_{\mathrm{eff}}(z)(z-a/2-L_z/2)\right]}{\cosh\left[M_{\mathrm{eff}}(z)(z+a/2-L_z/2)\right]}\,. \tag{8.2}$$

In order to define effective amplitudes we divide the data by a function with the fitted mass value (M_{fit}) inserted into eq. (8.1):

$$A_{\mathrm{eff}}(z) = G(z)\,\frac{\sinh[M_{\mathrm{fit}}L_z/2]}{\cosh[M_{\mathrm{fit}}(z-L_z/2)]}\,. \tag{8.3}$$

JHEP05(2014)117

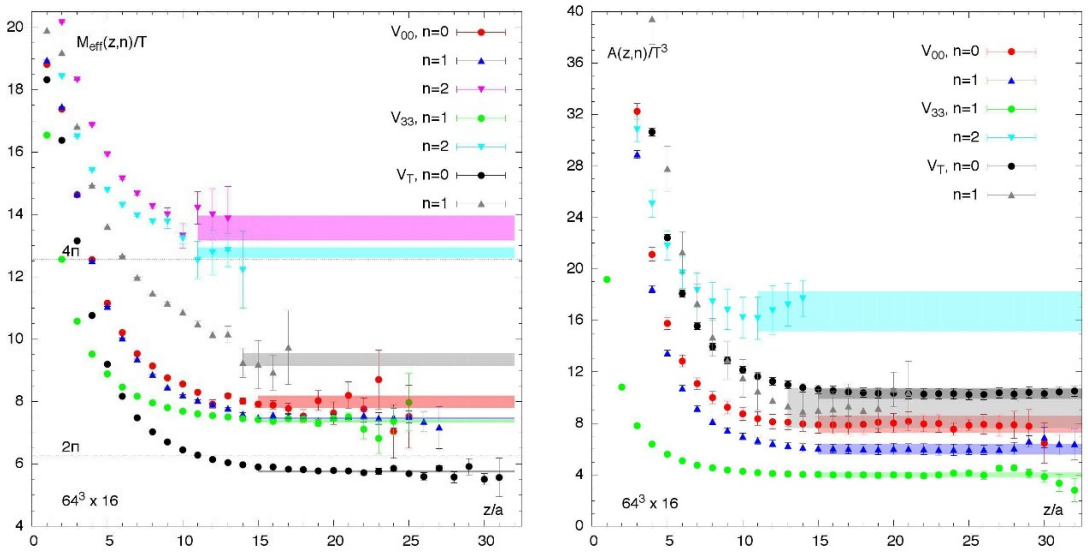

Figure 4. Examples of effective masses (left) and effective amplitudes (right) for the lattice 16×64^3 (the corresponding definitions are given in eqs. (8.2), (8.3)). The results are collected in table 3.

The results are shown for the lower temperature $T = 254(4)\,\mathrm{MeV}$ in figure 4. Like before, we refer to the screening masses in the following as "energies" ($M_{\rm fit} \to E$).

For $n \neq 0$ a non-trivial crosscheck on the overall procedure can be obtained through Ward identities. Given the complex nature of the fitting procedure and the fact that the lattice correlator measured is of a local-conserved type (cf. appendix B), the Ward identities are not trivially fulfilled. They assert that $E_{00}^{(n=1)} = E_{33}^{(n=1)}$ and that $k_n^2 A_{00}^{(n=1)} = [E_{33}^{(n=1)}]^2 A_{33}^{(n=1)}$. Using the average of $E_{00}^{(n=1)}$ and $E_{33}^{(n=1)}$ on the right-hand side we find for the ratio of the two sides 1.08(10) at $T = 254(4)\,\mathrm{MeV}$ and 1.15(7) at $T = 338(5)\,\mathrm{MeV}$, which indeed are consistent with unity within $\sim 2\sigma$ errors. The same consistency check is passed by the lattice data in the $n = 2$ sector.

8.3 Results and comparisons with perturbative predictions

Our final results for the screening masses are shown in figure 5, where they are also compared with the perturbative ones from table 2. The evolution of the perturbative results in the non-static sector when going from LO to EQCD results is illustrated in figure 6. The final lattice results for the screening masses and amplitudes are collected in table 3.

The following observations can be made:

- On a rough level, the free-theory predictions $E^{(n=0)} = k_1$, $E^{(n>0)} = k_n$ can be recognized in the full lattice data, with deviations that are $\lesssim 50\%$ (cf. figure 5).

- More quantitatively, for $n \neq 0$ the lattice and perturbative screening masses differ in general by less than 10% (cf. figure 5). A fairly good agreement is also observed for the P-wave screening mass in the static sector ($E_{00}^{(n=0)}$).

JHEP05(2014)117

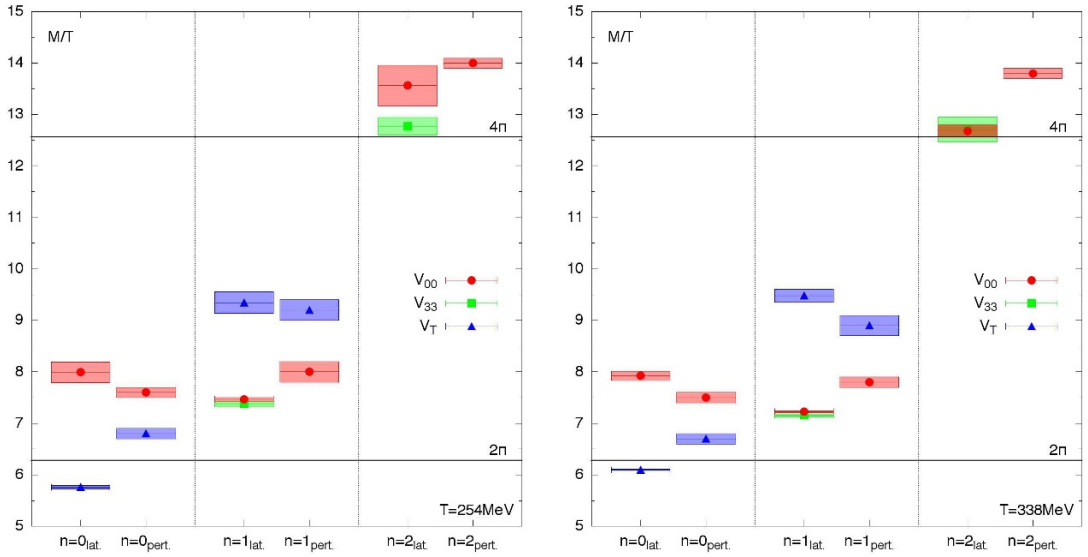

Figure 5. The lattice screening masses at $T = 254(4)\,\mathrm{MeV}$ (left) and $T = 338(5)\,\mathrm{MeV}$ (right), compared with the corresponding weak-coupling or effective-theory results from table 2. Note that discretization effects are expected to be larger at the higher temperature (i.e. $N_\tau = 12$), because then the distance scale $1/(4\pi T) = aN_\tau/(4\pi)$ is close to the lattice spacing.

- The S-wave screening masses in the static sector ($E_T^{(n=0)}$) differ by about 15% at the lower temperature, by 10% at the higher one. Although not large per se, such discrepancies are beyond the estimated systematic errors of the effective description. We recall, however, that in the static sector only the LO potential is known, so that an additional approximation has been made: in the language of the introduction these predictions are of type (i) rather than (ii).

- The splitting between the two S-wave masses ($E_{00}^{(n=1)} - E_T^{(n=0)}$) is reproduced very well, particularly at the higher temperature. It may be noted that at LO, the splitting is entirely due to the difference in the sign of the force from the A_0 exchange, represented by the function $K_0(m_{\mathrm{E}}y)$ in eqs. (6.12) and (6.31).

- The "amplitudes" do not compare well with each other: for the S-wave cases ($A_T^{(n=0)}$, $A_{00}^{(n=1)}$) the difference is $\sim 30\%$, but for the P-wave cases ($A_{00}^{(n=0)}$, $A_T^{(n=1)}$) it is much larger (cf. tables 2, 3). For $n = 2$ the difference is large even in the S-wave ($A_{00}^{(n=2)}$), and we get no signal in the P-wave ($A_T^{(n=2)}$). The amplitudes may however be expected to suffer from larger systematic uncertainties than the screening masses. On the perturbative side, we have determined the correlators only to LO as far as the amplitudes are concerned, not to NLO like for the screening masses. Moreover, the LO result arises from a numerical solution of the wave function and is thereby sensitive to soft scales, yet for heavy states the effective theory description of the soft dynamics is likely to be less accurate than for the ground state. On the lattice side, the amplitudes could be overestimated by misjudging where the plateau starts (put another way, they could include contributions from almost degenerate excited states). In

JHEP05(2014)117

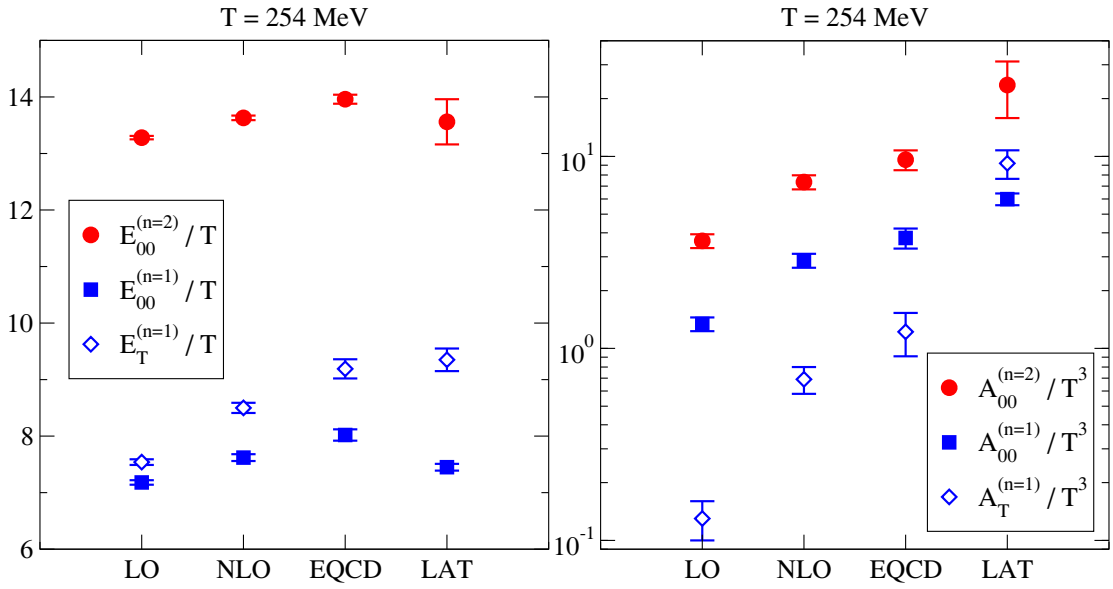

Figure 6. Left: a comparison of the perturbative (LO, NLO, EQCD, referring to whether the potential V^+ is from eq. (6.12), ref. [9], or ref. [10], respectively) and lattice (LAT) results for the non-static screening masses at $T = 254\,\mathrm{MeV}$. Right: the same for the corresponding amplitudes. Going from LO to EQCD yields in most cases an improvement, particularly for the amplitudes.

addition, discretization effects have not been estimated, given that we only consider a single lattice spacing. For all of these reasons we think that the $\sim 30\%$ discrepancy in the S-wave cases at $n = 0, 1$ is a reasonable reflection of the systematic uncertainties of a perturbative LO computation at the temperatures considered, whereas little can be deduced from the amplitudes related to the heavy states (P-wave or $n \geq 2$).

- The $\sim 30\%$ resolution in the S-wave cases at $n = 1$ ($A_{00}^{(n=1)}$) could only be reached thanks to the availability of the non-perturbative EQCD potential. Had only the LO potential been available, the discrepancy would have been $\sim 75\%$, cf. figure 6(right).

- Finally, we point out that in principle there is a "two-meson" threshold in each sector of fixed n. This physics has not been included in the current effective-theory analysis, however we believe that the states we have measured are light enough not to be affected.

9 Conclusions

We have considered mesonic screening masses related to the vector current both in a "static" (zero Matsubara frequency) and "non-static" (non-zero Matsubara frequency) sector. It turns out that even though in the weak-coupling limit both sectors probe physics at the momentum scale gT and can be represented by "non-relativistic" low-energy effective theories in $2+1$ dimensions, the physical significances of the sectors are different. Indeed only the non-static sector has a clear relation to real-time physics: we have

JHEP05(2014)117

shown that the potential appearing in the effective description (cf. eq. (6.12)) is identical to that previously considered in the context of jet quenching and photon and dilepton production in thermal QCD (cf. e.g. refs. [9]–[11]). On a general level, this observation is consistent with the statement that only non-zero Matsubara modes play a role in analytic continuation from imaginary to real time [32].

Apart from computing screening masses with an effective theory, we have also measured them with large-scale lattice Monte Carlo simulations in two-flavour QCD at temperatures of about 250 MeV and 340 MeV. We find a remarkably good agreement in the non-static sector, and also in the static sector for P-channel screening masses (cf. figure 5). This adds confidence to the applicability of effective theory methods for the study of phenomenologically interesting observables in the temperature range relevant for heavy ion collision experiments. (For "amplitudes" the agreement is poorer than for screening masses, but they also suffer from larger systematic errors both on the perturbative and on the lattice side, as has been discussed around the end of section 8.)

A general lesson, based on figure 2, is that higher-order corrections from the momentum scales gT and g^2T/π, even though formally suppressed by powers of g, are numerically of order 100% compared with results from the LO potential. In the case of the non-static sector we can at least partly account for these corrections, thanks to NLO computations and lattice simulations carried out in the context of jet quenching [9, 10]. Including these corrections in the solution of the Schrödinger equation indeed improves the overall agreement with lattice data (cf. figure 6).

In the case of the static sector, in contrast, the potential is different and no NLO or non-perturbative results exist for the moment. It seems conceivable, however, that computing such corrections might permit to reduce discrepancies between weak-coupling predictions and S-channel lattice data in the static sector. (The situation in the vector channel, illustrated in figure 5, is not too bad, however the discrepancy is larger in the scalar and pseudoscalar channels, cf. refs. [14, 15] and references therein.) Part of the discrepancy may be due to non-potential effects and spin-dependent terms, but it should be possible to incorporate these in the low-energy description as well.

In the present paper, we have demonstrated the existence of a relation between screening masses and real-time rates through perturbative arguments, employing four-dimensional lattice simulations only as a crosscheck for the accuracy of the perturbative description in the temperature range considered. It would be very interesting if similar relations could be established on a non-perturbative level. As a modest step in this direction, we may note that measuring the screening mass related to the operator $\int_0^{1/T} \mathrm{d}\tau\, e^{ik_n\tau}\, \bar{\psi}(\tau, \frac{\mathbf{y}}{2}, z)\, \gamma_0\, W_{\mathbf{y},z}\, \psi\big(\tau, -\frac{\mathbf{y}}{2}, z\big)$ directly in four dimensions, for k_n large, and cancelling the free behaviour through an exponential factor $\exp(k_n z)$ like in eq. (7.1), would allow us to define fully non-perturbative variants of the potential V^+ of eq. (7.6).

Acknowledgments

We acknowledge the use of computing time on the JUGENE computer of the Gauss Centre for Supercomputing (FZ Jülich, Germany); the $N_\tau = 16$ lattice ensemble was

JHEP05(2014)117

generated within the John von Neumann Institute for Computing (NIC) project HMZ21. The $N_\tau = 12$ ensemble was generated on the dedicated QCD platform "Wilson" at the Institute for Nuclear Physics, University of Mainz, whereas the correlation functions were computed on the "Clover" platform at the Helmholtz-Institute Mainz. The work of M.L was partly supported by the SNF under grant 200021-140234, and the work of H.M by the *Center for Computational Sciences in Mainz* as part of the Rhineland-Palatinate Research Initiative and by the DFG under grant ME 3622/2-1 *Static and dynamic properties of QCD at finite temperature.*

A Higher modes ($|n| > 1$)

In section 6, results obtained from the effective theory description were crosschecked against the free QCD results of section 3 for $n = 0, 1$. For completeness, we show here that the results match also for a general $|n| > 1$.

Expanding eqs. (3.8), (3.9) for a general k_n at $z \gg 1/|k_n|$, we obtain the asymptotics

$$G_{00}^{(k_n)}(z) = -N_c T^2 \frac{e^{-|k_n|z}}{z} \frac{2n^2+1}{6} + \mathcal{O}\left(\frac{e^{-|k_n|z}}{z^2}\right), \tag{A.1}$$

$$G_{T}^{(k_n)}(z) = -N_c T^2 \frac{e^{-|k_n|z}}{z^2} \frac{4n^2-1}{3|k_n|} + \mathcal{O}\left(\frac{e^{-|k_n|z}}{z^3}\right). \tag{A.2}$$

The qualitative behaviours are the same as in eqs. (3.10), (3.11), however there is a peculiar dependence on n. This is related to a non-trivial "degeneracy" of configurations leading to the same exponential fall-off at tree-level.

Consider a decomposition $k_n = p_n + (k_n - p_n)$, with $0 < p_n < k_n$. By making use of the free value $M_{\rm cm} = k_n$ (cf. eq. (6.6)), eqs. (6.10) and (6.26) read

$$\rho_{00,\rm LO}^{(k_n)}(\omega) = -N_c T \sum_{0<p_n<k_n} \left(\frac{1}{p_n} + \frac{1}{k_n - p_n}\right)^{-1} \theta(\omega - k_n), \tag{A.3}$$

$$\rho_{T,\rm LO}^{(k_n)}(\omega) = -N_c T \sum_{0<p_n<k_n} \left[\frac{1}{p_n^2} + \frac{1}{(k_n-p_n)^2}\right] \left(\frac{1}{p_n} + \frac{1}{k_n - p_n}\right)^{-2} (\omega - k_n)\,\theta(\omega - k_n). \tag{A.4}$$

The sums can be carried out:

$$\sum_{0<p_n<k_n} \left(\frac{1}{p_n} + \frac{1}{k_n - p_n}\right)^{-1} = \pi T \frac{2n^2+1}{6}, \tag{A.5}$$

$$\sum_{0<p_n<k_n} \left[\frac{1}{p_n^2} + \frac{1}{(k_n-p_n)^2}\right] \left(\frac{1}{p_n} + \frac{1}{k_n - p_n}\right)^{-2} = \frac{4n^2-1}{6n}. \tag{A.6}$$

We observe the same prefactors as in the full QCD results of eqs. (A.1), (A.2). Carrying out the Laplace transform in eq. (2.4) the overall coefficients can be seen to agree as well.

JHEP05(2014)117

B Technical details related to lattice simulations

Our simulations are based on the standard Wilson gauge action, with fermions implemented via the O(a) improved Wilson discretization with a non-perturbatively determined clover coefficient $c_{\rm sw}$ [33]. The configurations were generated with the MP-HMC algorithm [34, 35] employing the implementation of ref. [36] based on Lüscher's DD-HMC package [37].

Spatial correlation functions were computed on two ensembles, using the same discretization and masses as in the sea sector. The first ensemble, with a spatial size $N_s^3 = 64^3$ and a temporal extent of $N_\tau = 16$, consisted of 313 independent configurations. It was first presented in ref. [38] and has subsequently been analyzed in refs. [13, 39]. The second ensemble is newly generated, and has 262 configurations on an $N_\tau \times N_s^3 = 12 \times 64^3$ lattice. Both ensembles were generated at fixed bare parameters, corresponding to a lattice spacing $a = 0.0486(4)(5)$fm [28] so that $am_\pi N_s = 4.2$. Inserting into $T = 1/(N_\tau a)$ the two ensembles correspond to $T = 254(4)\,$MeV at $N_\tau = 16$ and $T = 338(5)\,$MeV at $N_\tau = 12$.

As in ref. [13], we implemented the vector correlation function as a mixed correlator between a local and a conserved current. The three correlators considered are

$$G_T^{(k_n)\rm bare}(z) \;=\; -a^3 \sum_{i,\tau,\mathbf{x}} e^{ik_n\tau} \left\langle\, J_i^c(\tau,\mathbf{x},z)\, J_i^l(0) \,\right\rangle , \tag{B.1}$$

$$G_{00}^{(k_n)\rm bare}(z) \;=\; -a^3 \sum_{\tau,\mathbf{x}} e^{ik_n\tau} \left\langle\, J_0^c(\tau,\mathbf{x},z)\, J_0^l(0) \,\right\rangle , \tag{B.2}$$

$$G_{33}^{(k_n)\rm bare}(z) \;=\; +a^3 \sum_{\tau,\mathbf{x}} e^{ik_n\tau} \left\langle\, J_3^c(\tau,\mathbf{x},z)\, J_3^l(0) \,\right\rangle , \tag{B.3}$$

where minus signs have been inserted in order to obtain positive correlators. The local (l) and conserved (c) currents are defined as ($x \equiv (\tau,\mathbf{x},z)$)

$$J_\mu^l(x) \equiv \frac{1}{\sqrt{2}}\, \bar{q}(x)\, \gamma_\mu\sigma_3\, q(x) \;, \tag{B.4}$$

$$J_\mu^c(x) \equiv \frac{1}{2\sqrt{2}} \Big[\bar{q}(x+a\hat{\mu})\,(1+\gamma_\mu) U_\mu^\dagger(x)\sigma_3\, q(x) - \bar{q}(x)\,(1-\gamma_\mu) U_\mu(x)\sigma_3\, q(x+a\hat{\mu}) \Big] \;. \tag{B.5}$$

Here q represents a mass-degenerate quark doublet, σ_3 a diagonal Pauli matrix acting on flavour indices, and U_μ a link matrix. The doublet can be interpreted as the u and d quarks.

In order to enhance the statistical precision of the measurements, we supplement the standard source at position $x_{\rm src} = 0$ with $N_{\rm src} = 64$ additional randomly chosen source positions in the lattice four-volume, thus obtaining $\lesssim 1\%$ statistical errors for the S-wave masses.

The local (non-conserved) vector current J_μ^l requires a finite renormalization factor $Z_{\rm V}$ (cf. e.g. ref. [40]). Correspondingly the bare vector correlators were renormalized using

$$G_{\mu\nu}^{(k_n)}(z) = Z_{\rm V}(g_0^2)\, G_{\mu\nu}^{(k_n)\rm bare}(z) \;, \tag{B.6}$$

with the non-perturbative value $Z_{\rm V}(g_0^2) = 0.768(5)$ at $6/g_0^2 = 5.50$ [41]. We have not included O(a) contributions from the improvement term proportional to the derivative of the antisymmetric tensor operator [42, 43], nor a quark-mass dependent improvement

JHEP05(2014)117

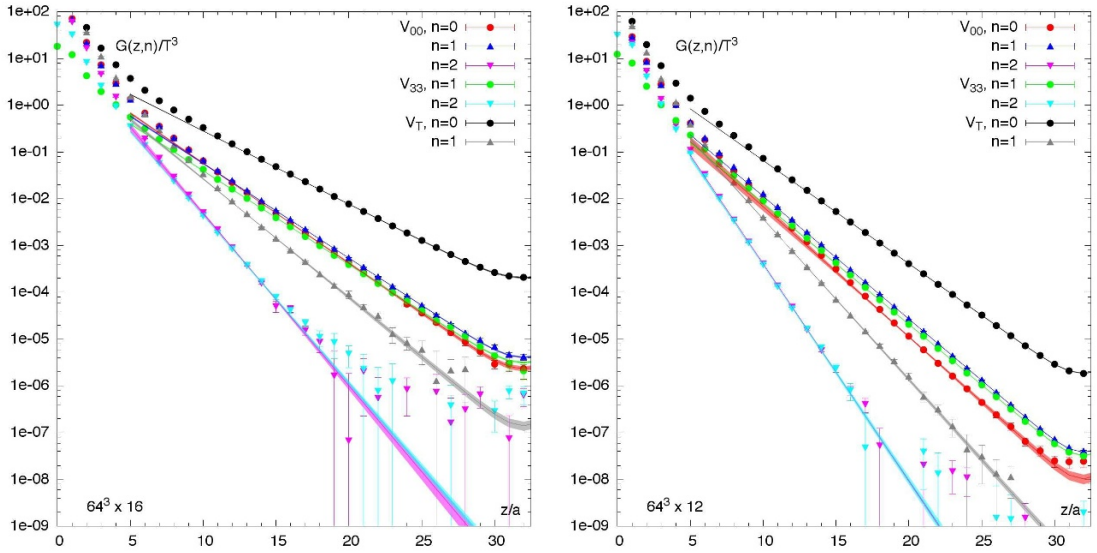

Figure 7. The correlators defined in eqs. (B.1)–(B.3), renormalized according to eq. (B.6), at $T = 254(4)\,\mathrm{MeV}$ (left panel) and $T = 338(5)\,\mathrm{MeV}$ (right panel). The shaded bands represent the fitted results with the corresponding ground state masses.

of the form $1 + b_{\mathrm{V}}(g_0^2)am_q$ [43]. Both should be included to ensure a smooth scaling behaviour as the continuum limit is taken, however our present study concerns a single (fine) lattice spacing.

The renormalized lattice data as well as the fitted correlation functions for the ground states are shown as the coloured shaded bands in figure 7. The error estimates were obtained via a jackknife procedure.

References

[1] D.J. Gross, R.D. Pisarski and L.G. Yaffe, *QCD and instantons at finite temperature*, *Rev. Mod. Phys.* **53** (1981) 43 [INSPIRE].

[2] J.I. Kapusta, *Quantum Chromodynamics at high temperature*, *Nucl. Phys.* **B 148** (1979) 461 [INSPIRE].

[3] T. Toimela, *The next term in the thermodynamic potential of QCD*, *Phys. Lett.* **B 124** (1983) 407 [INSPIRE].

[4] A.D. Linde, *Infrared problem in thermodynamics of the Yang-Mills gas*, *Phys. Lett.* **B 96** (1980) 289 [INSPIRE].

[5] P.H. Ginsparg, *First order and second order phase transitions in gauge theories at finite temperature*, *Nucl. Phys.* **B 170** (1980) 388 [INSPIRE].

JHEP05(2014)117

[6] T. Appelquist and R.D. Pisarski, *High-temperature Yang-Mills theories and three-dimensional Quantum Chromodynamics*, *Phys. Rev.* **D 23** (1981) 2305 [INSPIRE].

[7] H.B. Meyer, *Transport properties of the quark-gluon plasma: a lattice QCD perspective*, *Eur. Phys. J.* **A 47** (2011) 86 [arXiv:1104.3708] [INSPIRE].

[8] A. Hart, M. Laine and O. Philipsen, *Static correlation lengths in QCD at high temperatures and finite densities*, *Nucl. Phys.* **B 586** (2000) 443 [hep-ph/0004060] [INSPIRE].

[9] S. Caron-Huot, *$O(g)$ plasma effects in jet quenching*, *Phys. Rev.* **D 79** (2009) 065039 [arXiv:0811.1603] [INSPIRE].

[10] M. Panero, K. Rummukainen and A. Schäfer, *A lattice study of the jet quenching parameter*, *Phys. Rev. Lett.* **112** (2014) 162001 [arXiv:1307.5850] [INSPIRE].

[11] P. Aurenche, F. Gelis, G.D. Moore and H. Zaraket, *Landau-Pomeranchuk-Migdal resummation for dilepton production*, *JHEP* **12** (2002) 006 [hep-ph/0211036] [INSPIRE].

[12] M. Laine and M. Vepsäläinen, *Mesonic correlation lengths in high temperature QCD*, *JHEP* **02** (2004) 004 [hep-ph/0311268] [INSPIRE].

[13] B.B. Brandt, A. Francis and H.B. Meyer, *Antiscreening of the Ampere force in QED and QCD plasmas*, *Phys. Rev.* **D 89** (2014) 034506 [arXiv:1310.5160] [INSPIRE].

[14] O. Kaczmarek, E. Laermann and M. Müller, *The thermodynamic and the continuum limit of meson screening masses*, arXiv:1311.3889 [INSPIRE].

[15] S. Gupta and N. Karthik, *UV suppression by smearing and screening correlators*, arXiv:1311.4959 [INSPIRE].

[16] P.B. Arnold and C.-X. Zhai, *The three loop free energy for high temperature QED and QCD with fermions*, *Phys. Rev.* **D 51** (1995) 1906 [hep-ph/9410360] [INSPIRE].

[17] J. Möller and Y. Schröder, *Open problems in hot QCD*, *Nucl. Phys. Proc. Suppl.* **205-206** (2010) 218 [arXiv:1007.1223] [INSPIRE].

[18] W. Florkowski and B.L. Friman, *Spatial dependence of the finite temperature meson correlation function*, *Z. Phys.* **A 347** (1994) 271 [INSPIRE].

[19] M. Laine, M. Vepsäläinen and A. Vuorinen, *Intermediate distance correlators in hot Yang-Mills theory*, *JHEP* **12** (2010) 078 [arXiv:1011.4439] [INSPIRE].

[20] S.-Z. Huang and M. Lissia, *The dimensionally reduced effective theory for quarks in high temperature QCD*, *Nucl. Phys.* **B 480** (1996) 623 [hep-ph/9511383] [INSPIRE].

[21] J.C. Taylor and S.M.H. Wong, *The effective action of Hard Thermal Loops in QCD*, *Nucl. Phys.* **B 346** (1990) 115 [INSPIRE].

[22] E. Braaten and R.D. Pisarski, *Simple effective Lagrangian for Hard Thermal Loops*, *Phys. Rev.* **D 45** (1992) 1827 [INSPIRE].

[23] H.A. Weldon, *Effective fermion masses of order gT in high temperature gauge theories with exact chiral invariance*, *Phys. Rev.* **D 26** (1982) 2789 [INSPIRE].

[24] W.M. Alberico, A. Beraudo, A. Czerska, P. Czerski and A. Molinari, *Meson screening masses in the interacting QCD plasma*, *Nucl. Phys.* **A 792** (2007) 152 [hep-ph/0703298] [INSPIRE].

[25] J. Ghiglieri et al., *Next-to-leading order thermal photon production in a weakly coupled quark-gluon plasma*, *JHEP* **05** (2013) 010 [arXiv:1302.5970] [INSPIRE].

JHEP05(2014)117

[26] M. D'Onofrio, A. Kurkela and G.D. Moore, *Renormalization of null Wilson lines in EQCD*, *JHEP* **03** (2014) 125 [arXiv:1401.7951] [INSPIRE].

[27] M. Laine and A. Rothkopf, *Towards understanding thermal jet quenching via lattice simulations*, arXiv:1310.2413 [INSPIRE].

[28] P. Fritzsch et al., *The strange quark mass and Λ parameter of two flavor QCD*, *Nucl. Phys.* **B 865** (2012) 397 [arXiv:1205.5380] [INSPIRE].

[29] B.B. Brandt, A. Francis, H.B. Meyer, O. Philipsen and H. Wittig, *QCD thermodynamics with $O(a)$ improved Wilson fermions at $N_{\rm f} = 2$*, arXiv:1310.8326 [INSPIRE].

[30] E. Braaten and A. Nieto, *Free energy of QCD at high temperature*, *Phys. Rev.* **D 53** (1996) 3421 [hep-ph/9510408] [INSPIRE].

[31] M. Laine and Y. Schröder, *Two-loop QCD gauge coupling at high temperatures*, *JHEP* **03** (2005) 067 [hep-ph/0503061] [INSPIRE].

[32] G. Cuniberti, E. De Micheli and G.A. Viano, *Reconstructing the thermal Green functions at real times from those at imaginary times*, *Commun. Math. Phys.* **216** (2001) 59 [cond-mat/0109175] [INSPIRE].

[33] ALPHA collaboration, K. Jansen and R. Sommer, *$O(a)$ improvement of lattice QCD with two flavors of Wilson quarks*, *Nucl. Phys.* **B 530** (1998) 185 [*Erratum ibid.* **B 643** (2002) 517] [hep-lat/9803017] [INSPIRE].

[34] M. Hasenbusch, *Speeding up the hybrid Monte Carlo algorithm for dynamical fermions*, *Phys. Lett.* **B 519** (2001) 177 [hep-lat/0107019] [INSPIRE].

[35] M. Hasenbusch and K. Jansen, *Speeding up lattice QCD simulations with clover improved Wilson fermions*, *Nucl. Phys.* **B 659** (2003) 299 [hep-lat/0211042] [INSPIRE].

[36] M. Marinkovic and S. Schaefer, *Comparison of the mass preconditioned HMC and the DD-HMC algorithm for two-flavour QCD*, PoS(LATTICE 2010)031 [arXiv:1011.0911] [INSPIRE].

[37] M. Lüscher, webpage *DD-HMC algorithm for two-flavour lattice QCD*, http://luscher.web.cern.ch/luscher/DD-HMC/index.html.

[38] B.B. Brandt, A. Francis, H.B. Meyer and H. Wittig, *Thermal correlators in the ρ channel of two-flavor QCD*, *JHEP* **03** (2013) 100 [arXiv:1212.4200] [INSPIRE].

[39] B.B. Brandt, A. Francis, H.B. Meyer and H. Wittig, *Two-flavour lattice QCD correlation functions in the deconfinement transition region*, PoS(Confinement X)186 [arXiv:1302.0675] [INSPIRE].

[40] QCDSF-UKQCD collaboration, T. Bakeyev et al., *Nonperturbative renormalization and improvement of the local vector current for quenched and unquenched Wilson fermions*, *Phys. Lett.* **B 580** (2004) 197 [hep-lat/0305014] [INSPIRE].

[41] M. Della Morte, R. Hoffmann, F. Knechtli, R. Sommer and U. Wolff, *Non-perturbative renormalization of the axial current with dynamical Wilson fermions*, *JHEP* **07** (2005) 007 [hep-lat/0505026] [INSPIRE].

[42] M. Lüscher, S. Sint, R. Sommer and P. Weisz, *Chiral symmetry and $O(a)$ improvement in lattice QCD*, *Nucl. Phys.* **B 478** (1996) 365 [hep-lat/9605038] [INSPIRE].

[43] S. Sint and P. Weisz, *Further results on $O(a)$ improved lattice QCD to one loop order of perturbation theory*, *Nucl. Phys.* **B 502** (1997) 251 [hep-lat/9704001] [INSPIRE].

JHEP05(2014)117